UNIVERSIDADE DE SÃO PAULO
INSTITUTO DE GEOCIÊNCIAS
PROGRAMA DE PÓS- GRADUAÇÃO EM GEOCIÊNCIAS (GEOQUÍMICA E GEOTECTÔNICA)

JAQUELINE QUIRINO FERREIRA

CHANGES IN HYDROCLIMATE AND VEGETATION IN THE SÃO FRANCISCO RIVER DRAINAGE BASIN DURING THE LAST 45000 YEARS

São Paulo
2021

JAQUELINE QUIRINO FERREIRA

CHANGES IN HYDROCLIMATE AND VEGETATION IN THE SÃO FRANCISCO RIVER DRAINAGE BASIN DURING THE LAST 45000 YEARS

Versão corrigida

Dissertação apresentada ao Programa de Pós-Graduação em Geociências (Geoquímica e Geotectônica) do Instituto de Geociências da Universidade de São Paulo como requisito para obtenção do título de Mestre em Ciências

Área de concentração:
Geoquímica dos Processos Exógenos

Orientador:
Prof. Dr. Cristiano Mazur Chiessi

São Paulo
2021

Serviço de Biblioteca e Documentação do IGc/USP
Ficha catalográfica gerada automaticamente com dados fornecidos pelo(a) autor(a)
via programa desenvolvido pela Seção Técnica de Informática do ICMC/USP

Bibliotecários responsáveis pela estrutura de catalogação da publicação:
Sonia Regina Yole Guerra - CRB-8/4208 | Anderson de Santana - CRB-8/6658

Quirino Ferreira, Jaqueline
CHANGES IN HYDROCLIMATE AND VEGETATION IN THE SÃO FRANCISCO RIVER DRAINAGE BASIN DURING THE LAST 45000 YEARS / Jaqueline Quirino Ferreira; orientador Cristiano Mazur Chiessi. -- São Paulo, 2021.
60 p.

Dissertação (Mestrado - Programa de Pós-Graduação em Geoquímica e Geotectônica) -- Instituto de Geociências, Universidade de São Paulo, 2021.

1. Quaternary. 2. South America. 3. vegetation. 4. orbital forcing . 5. long chain n-alkanes. I. Mazur Chiessi, Cristiano , orient. II. Título.

UNIVERSIDADE DE SÃO PAULO
INSTITUTO DE GEOCIÊNCIAS

Changes in hydroclimate and vegetation in the São Francisco River drainage basin during the last 45000 years

JAQUELINE QUIRINO FERREIRA

Orientador: Prof. Dr. Cristiano Mazur Chiessi

Dissertação de Mestrado

Nº 866

COMISSÃO JULGADORA

Dr. Cristiano Mazur Chiessi

Drª. Raquel Franco Cassino

Drª. Marina Hirota Magalhães

SÃO PAULO
2021

ACKNOWLEDGEMENTS

I thank Prof. Dr. Cristiano M. Chiessi for supervising me and for all the opportunities and dedication. The immense support offered by him was of fundamental importance for my academic development and for accomplishing this study.

I thank my colleagues at the Paleoceanography and Paleoclimatology Laboratory (P2L) at the School of Arts, Sciences and Humanities, and the Institute of Geosciences for interesting academic discussions and meetings. Special thanks go to Dr. Marília Campos for the support, as well as to Dr. Dailson Bertassoli and MSc. Thomas Akabane for the company during the fieldtrip in the São Francisco River Basin - crossing this river from its headlands to its mouth was an unforgettable experience.

I thank my supervisor abroad, Dr. Enno Schefuß for his patience and help. Special thanks go to Ralph Kreutz for the technical support. I also thank all my colleagues at the MARUM – Center of Marine Environmental Science (University of Bremen, Germany) who helped me with laboratory procedures. Many thanks go to MSc. Débora Raposo and MSc. Jéssica Resende for the helping me during my stay in Bremen.

I am grateful to the infrastructure of the University of São Paulo that made possible my Master's degree. I thank CAPES for the MSc. scholarship (grant 88882.328049/2019-01), as well as for two grants that partially financed this study (grants 564/2015 and 88881.313535/2019-01). Other funding agencies are also thanked for partially financing this study: FAPESP (grants 2013/50297-0, 2018/15123-4 and 2019/24349-9), CNPq (grants 302607/2016-1 and 422255/2016-5) and the Alexander von Humboldt Foundation. I thank the captain and crew of RV Meteor cruise M125 for support during sampling.

Finally, I thank my family for everything. My deepest thanks go to my husband, Leonardo M., who has supported me immensely both in my studies and personal journey over the past decade.

ABSTRACT

Ferreira, J.Q, **Changes in hydroclimate and vegetation in the São Francisco River Drainage Basin during the last 45000 years.** [Master's Thesis], São Paulo, Instituto de Geociências, Universidade de São Paulo, 2021. 60 pp.

The São Francisco River Drainage Basin is the larger hydrographic system in eastern South America. This basin has a huge ecological importance due to its extension and because it hosts a large portion of Cerrado (a type of tropical savanna), as well as Caatinga and, subordinately, Atlantic Forest. Despite that, the main factors that controlled changes in the biomes during the last tens of thousands of years and were, at least partially, responsible for their current distribution are still largely unknown. This is due to the small number of long paleoenvironmental reconstructions that integrate large areas of the São Francisco River basin. Here, we used the stable hydrogen (δD) and carbon ($\delta^{13}C$) isotope composition of long-chain *n*-alkanes from a marine sediment core to reconstruct past hydroclimate and vegetation, respectively, in an independent way. Long-chain *n*-alkanes are plant-wax biomarkers present in the wax coating of leaves. δD values of plant-waxes register the isotope composition of meteoric water, which is, in turn, controlled by the amount effect in the tropics. Hence, the δD of plant-waxes can be used to reconstruct past precipitation. $\delta^{13}C$ values of plant-waxes allows the differentiation between vegetation types using the C3 and C4 photosynthetic pathways. Since tropical forest taxa mostly use the C3 metabolisms, while tropical savanna taxa predominantly use the C4 metabolism, this method allows to study potential shifts in the dominant vegetation type. To do so, we analyzed marine sediment core M125-95-3 collected from the western tropical South Atlantic (10.94ºS, 36.20ºW, 1897 m water depth, 1040 cm core length), near the mouth of the São Francisco River, spanning the last 45 kyr. On top of millennial-scale changes, $\delta^{13}C$ data indicate for the first time a marked obliquity control over the proportion of trees (C3) versus grasses (C4). During periods of maximum (minimum) obliquity, trees (grasses) reached maximum coverage. Importantly, our δD record does not indicate orbital-scale changes in precipitation. We suggest that maximum (minimum) obliquity decreased (increased) the length of the dry season allowing (hampering) the development of trees. Periods of maximum (minimum) obliquity increased (decreased) the intra-hemispheric insolation gradient during austral winter, strengthening the austral Hadley circulation and the southeastern trade winds. Both processes slightly increased winter precipitation over the São Francisco River Drainage Basin, decreasing the length of the dry season. Our results suggest that the dry season length is a governing factor in the long-term control of tree density in tropical savannas.

Keywords: Quaternary; South America; vegetation; orbital forcing; long chain *n*-alkanes.

RESUMO

Ferreira, J.Q, **Mudanças no hidroclima e vegetação na Bacia do Rio São Francisco durante os últimos 45000 anos.** [Dissertação de Mestrado], São Paulo, Instituto de Geociências, Universidade de São Paulo, 2021. 60 pp.

A bacia hidrográfica do rio São Francisco é o maior sistema hidrográfico do leste da América do Sul. Esta bacia possui grande importância ecológica devido à sua extensão e por abrigar parte substancial do Cerrado (um tipo de savana tropical), além de amplas áreas de Caatinga e, subordinadamente, Mata Atlântica. Apesar disso, os principais fatores que controlaram as alterações nestes biomas durante as últimas dezenas de milhares de anos e foram, pelo menos em parte, responsáveis pela sua atual distribuição, são ainda amplamente desconhecidos. Isto se deve ao pequeno número de reconstituições paleoambientais longas que integrem extensas áreas da bacia do rio São Francisco. Neste estudo a composição dos isótopos estáveis de hidrogênio (δD) e carbono ($\delta^{13}C$) de *n*-alcanos de cadeia longa de um testemunho sedimentar marinho foi usada para reconstituir a história geológica do hidroclima e da vegetação da bacia, respectivamente, de forma independente. *n*-Alcanos de cadeia longa são biomarcadores vegetais presentes no revestimento de cera das folhas. Os valores de δD de ceras vegetais refletem a composição isotópica da água meteórica, que é controlada pelo "*amount effect*" nos trópicos. Dessa forma, δD de ceras vegetais pode ser usado para reconstituir a precipitação pretérita. Já os valores de $\delta^{13}C$ de ceras vegetais permitem diferenciar os tipos de vegetação usando as vias fotossintéticas C3 e C4. Uma vez que táxons de floresta tropical usam principalmente o metabolismo C3, enquanto que os táxons de savana tropical usam principalmente o metabolismo C4, este método permite reconstituir mudanças potenciais no tipo de vegetação dominante. Para isso, analisamos o testemunho sedimentar marinho M125-95-3 coletado na porção oeste do Atlântico Sul tropical (10,94ºS, 36,20ºW, lâmina d'água de 1897 m, 1040 cm de comprimento), próximo à foz do rio São Francisco, abrangendo os últimos 45 kyr. Em adição às mudanças milenares, os dados de $\delta^{13}C$ mostram pela primeira vez o controle da obliquidade sobre a proporção de árvores (C3) versus gramíneas (C4). Durante os períodos de obliquidade máxima (mínima), as árvores (gramíneas) atingiram a maior cobertura. O registro de δD, entretanto, não indica mudanças na precipitação na escala orbital. Sugere-se que a obliquidade máxima (mínima) diminuiu (aumentou) a duração da estação seca, permitindo (dificultando) a expansão da cobertura de árvores. Períodos de obliquidade máxima (mínima) aumentaram (diminuíram) o gradiente de insolação intrahemisférico durante o inverno austral, fortalecendo a circulação de Hadley do hemisfério sul e os ventos alísios de sudeste. Ambos processos aumentaram ligeiramente a precipitação de inverno austral na bacia do rio São Francisco, diminuindo a duração da estação seca. Nossos resultados sugerem que a duração da estação seca é um fator determinante no controle de longo prazo da densidade de árvores em savanas tropicais.

Palavras-chave: Quaternário; América do Sul; vegetação; forçante orbital; *n*-alcanos de cadeia longa.

TABLE OF CONTENTS

1 CHAPTER 1 15

1.1 INTRODUCTION 15

1.2 RESEARCH AIMS 19

2 CHAPTER 2 20

2.1 LONG CHAIN *n*-ALKANES 20

2.2 PALEOENVIRONMENTAL RECONSTRUCTIONS IN EASTERN SOUTH AMERICA 26

3 CHAPTER 3 32

3.1 ABSTRACT 32

3.2 INTRODUCTION 33

3.3 REGIONAL SETTING 34

3.4 MATERIAL AND METHODS 36

3.4.1 Marine sediment core and geoinformation 36

3.4.2 Age model 36

3.4.3 Lipids extraction and compound isolation 36

3.4.4 n-Alkane quantification 37

3.4.5 Compound-specific isotope analyses 37

3.4.6 Ice volume correction 38

3.4.7 Geoinformation processing 38

3.5 RESULTS 39

3.6 DISCUSSION 42

3.6.1 Orbital forcing 42

3.6.2 Millennial forcing 45

3.6.3 Ecological perspectives 45

3.7 CONCLUSIONS 46

3.8 ACKNOWLEDGEMENTS 47

3.9 SUPPLEMENTARY MATERIAL 48

4 CHAPTER 4 49

4.1 CONCLUSIONS 49

REFERENCES 50

LIST OF FIGURES

Figure 1.1 Precipitation charts for selected stations in the São Francisco São Francisco River Drainage Basin (note the different y-axis values). **A.** Fazenda Coqueiro (São Desidério/BA). **B.** Lagoa das Pedras (Montalvânia/MG). **C.** Barra do Escuro (São Romão/MG). **D**. IBO (Abaré/BA). **E.** Pão de Açúcar (Pão de Açúcar/AL). **F.** Jaguaruna – jusante (Onça de Pitangui/MG). Data obtained from Agência Nacional de Águas (ANA) ……………………………………………………………...……..............................……15

Figure 1.2 Distribution of biomes in eastern South America (IBGE, 2004). The location of marine sediment core M125-95-3 is indicated by a green circle …………………..…..…….17

Figure 2.1 Histogram showing normal distribution of bulk C3 and C4 plant isotopic values (Tipple & Pagani, 2007) ……...……………………………………......................………22

Figure 2.2 Box plots of δ^{13}C data from soil bulk organic matter available for the São Francisco River Drainage Basin and its direct neighborhood (Mendonça et al., 2010; Pessenda et al., 1996, 1998; 2010). The data for Cerrado and Forest are indicated by the green and orange box plots, respectively……………………………….…………..……………23

Figure 2.3 Relationships between source-water δD and lipid biomarker δD values from lake-surface sediment samples from Europe, Africa and the Americas (Sachse et al., 2012) …...25

Figure 2.4 Long term means (monthly) and associated standard deviation of δD (rainwater) obtained from Global Network of Isotopes in Precipitation database. Accessible at: https://nucleus.iaea.org/wiser. Data from Belo Horizonte (blue line and dot), Brasília (orange line and square) and Floresta (red line and triangle) stations………………...………..25

Figure 2.5 Location of selected palynological records (pink circles) from the São Francisco River Drainage Basin and its direct neighborhood, on top of the distribution of Brazilian biomes (IBGE, 2004). **1.** São José palm swamp (Cassino et al., 2018) **2.** Icatu River Valley (De Oliveira et al., 1999a) **3.** Lagoa Feia (Cassino et al., 2020) **4.** Chapadão dos Gerais

(Franco Cassino & Meyer, 2013) **5.** Pinheiro mire (Horák-Terra et al., 2020) **6.** Lagoa Nova (Behling, 2003) **7.** Salitre de Minas (Ledru, 1993). The location of the M125-95-3 marine core is indicated by the green circle in **8**………………………………………………29

Figure 2.6 Eastern South American paleoenvironmental records over the last ca. 35 kyr. **A.** Speleothems stable oxygen isotopic record ($\delta^{18}O$) from eastern Brazil (Stríkis et al., 2018). **B.** ln(Ti/Ca) data of core M125-95-3 (Campos et al., 2019). **C.** $\delta^{13}C$ from peat core Pinheiro mire (Horák-Terra et al., 2020). **D.** Obliquity values (Laskar et al., 2004). **E.** Arboreal pollen percentage (AP %) from Lagoa Feia (Cassino et al., 2020). **F.** AP% from Pinheiro mire (Horák-Terra et al., 2020). See Table 2.1 and Figure 2.5 for the location of the described records ……………………………………………………………………………………31

Figure 3.1 Climatological and ecological features of the São Francisco River Basin and adjacent areas. **A.** Dry season length (Funk et al., 2015) **B.** Distribution of tropical forest, savanna and grassland based on Mapbiomas land cover data (Souza et al., 2020) **C.** Mean annual precipitation (Harris et al., 2020). The black rectangle in C depicts the area shown in A and B. The location of marine sediment core M125-95-3 is indicated by a white circle. The location of the Lapa Grande and Lapa Sem Fim speleothem records are indicated by yellow circles in all subplots (Stríkis et al., 2018) ………………………………………………35

Figure 3.2 Stable hydrogen (δD) and carbon ($\delta^{13}C$) isotopic records of plant waxes from marine sediment core M125-95-3 for the last ca. 45 kyr. **A**. Ice volume corrected δD_{29} (dashed line) and δD_{31} (continuous line) values recording changes in precipitation over the São Francisco River Drainage Basin (SFRB). **B.** $\delta^{13}C_{29}$ (dashed line) and $\delta^{13}C_{31}$ (continuous line) values recording changes in the relative abundance of C3 versus C4 vegetation in the SFRB. Calibrated ^{14}C accelerator mass spectrometry ages with 2 sigma error of core M125-95-3 are indicated by triangles on the lower axis. The grey bars indicate Heinrich Stadials (HS) 4 to 1. Marine Isotope Stages (MIS) are depicted on top of panel A. Shaded areas in the isotope records indicate the standard deviation of isotope values based on standard measurements ………………………………………………………………………………………………40

Figure 3.3 Precipitation and vegetation reconstructions for the São Francisco River Drainage Basin for the last ca. 45 kyr. **A**. Speleothem stable oxygen isotopic record ($\delta^{18}O$) from eastern Brazil (Stríkis et al., 2018). **B**. Plant waxes stable hydrogen isotopic record (δD_{wax}) of marine sediment core M125-95-3 representing average values between C_{29} and C_{31} *n*-alkanes (blue continuous line) (this study); ln(Ti/Ca) data of core M125-95-3 (dotted black line) (Campos et al., 2019). **C**. Austral summer (December-February) insolation values for 15ºS (Laskar et al., 2004); obliquity values (Laskar et al., 2004). **D.** Plant waxes stable carbon isotopic record ($\delta^{13}C_{wax}$) of core M125-95-3 representing average values between C_{29} and C_{31} *n*-alkanes. Calibrated ^{14}C accelerator mass spectrometry ages with 2 sigma error of core M125-95-3 are indicated by triangles on the lower axis. The grey bar indicates the Heinrich Stadial (HS) 4 to 1. Marine Isotope Stages (MIS) are depicted on top of the panel A. Shaded areas in the isotope records indicate the standard deviation of isotope values……………………..……41

Figure 3.4 Distribution of the dry season length (DSL) (Funk et al., 2015) in tropical forest and savanna (i.e., savanna plus grasslands) domains (Souza et al., 2020) over eastern tropical South America (i.e., 7-22ºS, 48-36ºW), encompassing the São Francisco River Drainage Basin. **A.** Box plots of the DSL for tropical forest and savanna (i.e., savanna plus grasslands). **B.** Density plots of the DSL …..…………………………………………..……………42

Figure S1. Downcore records of the carbon preference index (CPI_{25-33}) and the average chain length (ACL_{25-33}) of marine sediment core M125-95-3 for the last ca. 45 kyr. Despite the low Holocene CPI_{25-33} values, the long-chain *n*-alkanes present in most of the record are predominantly derived from terrestrial higher plants (Cranwell, 1981) ………...……………..………48

LIST OF TABLES

Table 2.1 Selected palynological records from the São Francisco River Drainage Basin and its direct neighborhood. For the location of the records see Figure 2.5 ……………………………………………………..........………...………………..............…............30

1 CHAPTER 1

1.1 INTRODUCTION

The São Francisco River Drainage Basin (SFRB) is the larger river system in eastern South America. Starting in the Serra da Canastra at ca. 20°S (southeastern Brazil), the São Francisco River flows northwards until ca. 10°S, when it veers eastwards reaching the tropical South Atlantic around 10.5°S (Figure 1.1). The headlands of the SFRB are under the influence of the South Atlantic Convergence Zone (SACZ), a NW-SE oriented convective belt originating in the Amazon Basin that extends over southeastern South America and over the adjacent South Atlantic (Carvalho et al., 2004). The SACZ is a distinctive feature of the South American Monsoon System (SAMS), that dominates the seasonal precipitation cycle in South America (Vera et al., 2006; Zhou & Lau, 1998), which has its mature phase in austral summer (December-February) (Vera et al., 2006). Due to this influence, the headlands of the SFRB are wetter than the rest of the basin (Figure 1.1).

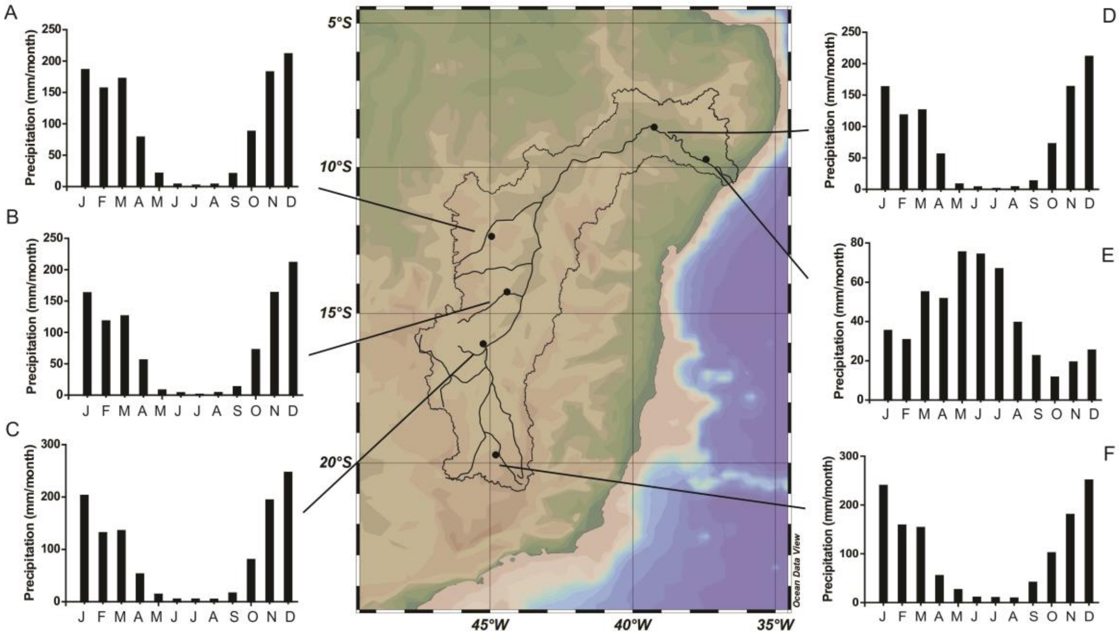

Figure 1.1 Precipitation charts for selected stations in the São Francisco River Drainage Basin (note the different y-axis values). **A.** Fazenda Coqueiro (São Desidério/BA, 1973 - 2018). **B.** Lagoa das Pedras (Montalvânia/MG, 1969-2018). **C.** Barra do Escuro (São Romão/MG, 1956-2018). **D**. IBO (Abaré/BA, 1969-2018). **E.** Pão de Açúcar (Pão de Açúcar/AL, 1935-2018). **F.** Jaguaruna – jusante (Onça de Pitangui/MG, 1942-2018). Data obtained from Agência Nacional de Águas (ANA).

The SAMS intensity is dominantly influenced by changes in austral summer insolation, that in turn is strongly associated with the precession cycle (period of ca. 23 ka) (Cheng et al., 2013; Cruz et al., 2005; Govin et al., 2014; Hou et al., 2020). In the upper-troposphere, the convective activity associated to the SAMS produces the Bolivian High over the Altiplano that is dynamically linked to the Nordeste Low over northeastern Brazil (Lenters & Cook, 1997). The Nordeste Low, in turn, produces large-scale subsidence over northeastern Brazil that affects the northern portion of the SFRB. In a precession-driven high austral summer insolation situation a strengthened SAMS intensifies this circulation pattern, increasing precipitation over the western Amazon and under the SACZ, as well aridity over northeastern Brazil (Cheng et al., 2013; Cruz et al., 2009).

Because of the opposing hydroclimatic influences over the southern and northern realms of the SFRB, speleothem-based precipitation records from the central portion of the SFBR show no clear precession-driven changes (Stríkis et al., 2018). These records, along with other studies (Campos et al., 2019; Stríkis et al., 2011), indicate that precipitation over this portion of eastern South America was strongly modulated by millennial-scale events. Based on data from marine sediment core M125-95-3 collected off the mouth of the SFRB, Campos et al. (2019) corroborated the lack of orbital-scale changes in hydroclimate and proposed that positive precipitation anomalies over the SFRB during the so-called Heinrich Stadials (HS) (Bond et al., 1992; Heinrich, 1988; Sanchez Goñi & Harrison, 2010) were associated with increased austral summer rainfall over eastern tropical South America. According to this mechanism, increased austral summer rainfall occurred due to an anomalous cyclonic circulation and moisture transport from the warmer South Atlantic into the continent.

The central SFRB hosts a large portion of Cerrado biome (Figure 1.2), a complex ecosystem with mixed trees and grasses, ranging from tree-less open vegetation (Campo Limpo) with a dense grassland ground, to a closed canopy with a dense occurrence of trees (Cerradão) and associated gallery forests following the watercourses (Bridgewater et al., 2004; Da Silva & Bates, 2002; Toby Pennington et al., 2000). The northern portion of the SFRB is covered by Caatinga formations (Figure 1.2) - a type of tropical dry forest, composed by xerophytic, woody, thorny and deciduous physiognomies (Sampaio, 1995). Atlantic Forest occurs over the southern portion of the SFRB and along a narrow coastal stripe close to the coast of northeastern Brazil (Figure 1.2) and is composed by two major vegetation types: the Atlantic Rain Forest, which runs along the coastline, and the Atlantic Semi-deciduous Forest, which occupies higher elevation inland areas (Oliveira-Filho & Fontes, 2000).

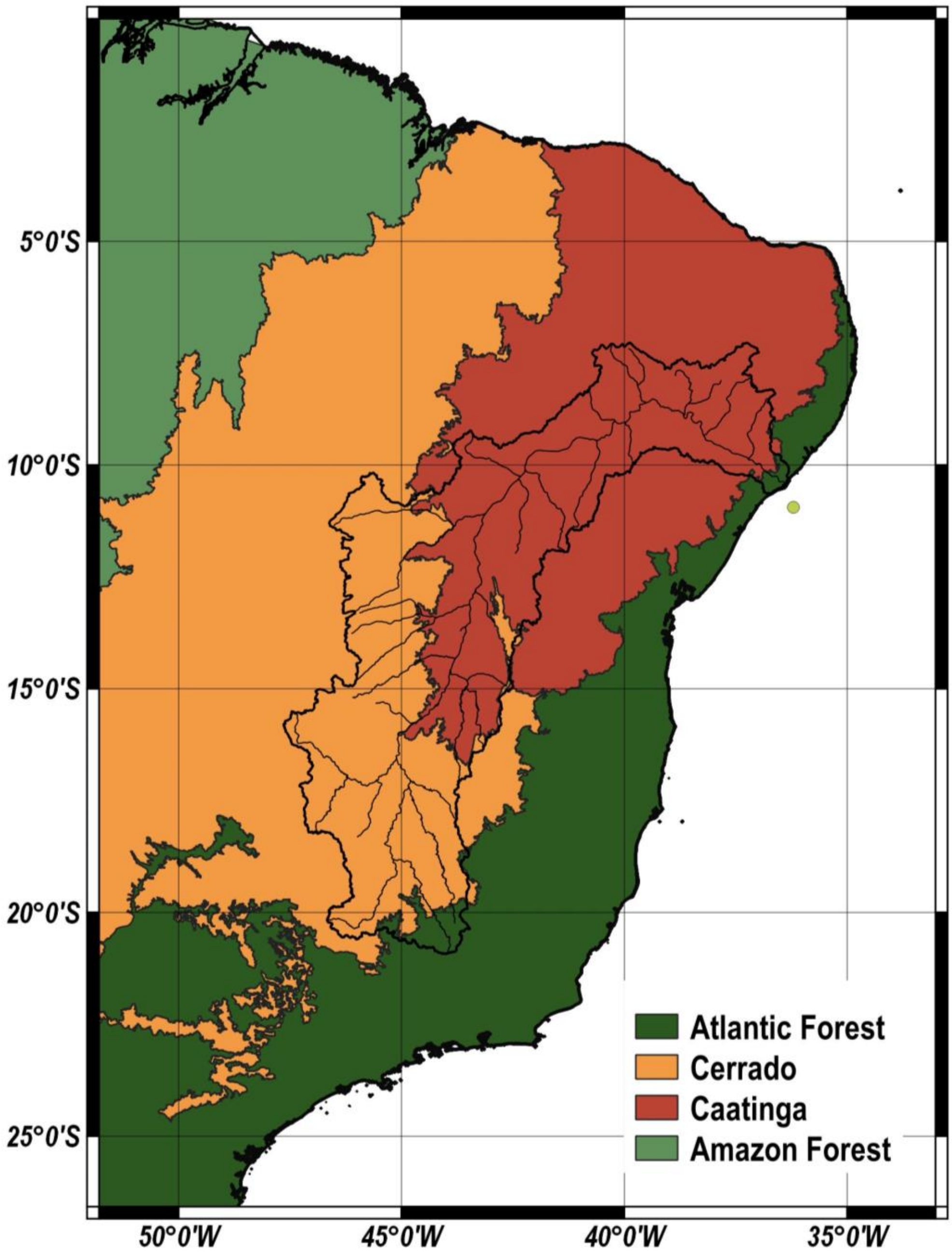

Figure 1.2 Distribution of biomes in eastern South America (IBGE, 2004). The location of marine sediment core M125-95-3 is indicated by the green circle.

Accurate reconstructions of hydroclimate and vegetational changes in this area are critical to understanding the potential influence of climate variability over tropical biogeography and biodiversity (Bouimetarhan et al., 2018; Dupont et al., 2010). Despite important efforts undertaken to reconstruct past dynamics of the Cerrado (Cassino et al., 2020; Cassino & Meyer, 2013; Horák-Terra et al., 2020), Caatinga (De Oliveira et al., 1999) and Tropical forest (Behling, 2003), available records are either short or have a localized meaning. Paleoenvironmental information from a marine sediment core integrating large portions of the SFRB, for instance, is largely missing.

Plant biomarkers have been recognized as an important tool to reconstruct past climatic and vegetational changes (Huang, 2001; Schefuß et al., 2011). Changes in environmental conditions are imprinted on the molecular residues of organisms that lived during different past times. Thus, the composition of compounds like lipids present in sediments record paleoenvironmental changes (Meyers, 1997). *n*-Alkanes are commonly used as paleoenvironmental signal carriers since they record past environmental conditions and present excellent preservation against degradation during transport and deposition (Diefendorf & Freimuth, 2017; Häggi et al., 2017).

Marine sediment core M125-95-3 (Bahr et al., 2016) collected off the SFRB mouth, was investigated within this Master's dissertation (Figure 1.2). The core covers the last ca. 45 kyr (Campos et al., 2019). We used the stable carbon ($\delta^{13}C$) and hydrogen (δD) isotopic composition of epicuticular waxes (i.e., long-chain *n*-alkanes) of terrestrial higher plants to reconstruct the main photosynthetic pathway of vegetation (i.e., C3 trees versus C4 grasses) and the amount of precipitation, respectively, over the SFRB. The performed analytical results, together with their interpretation, constitute a manuscript (Chapter 3) entitled "*Changes in obliquity drive biome shifts in eastern tropical South America*" (under submission). In this manuscript, we show evidence and describe how the dry season length is a governing factor in the long-term control of tree density in tropical savannas of the SFRB area.

In this dissertation, a review of *n*-alkanes and available paleoenvironmental records of interest to this study is provided in Chapter 2. A full description of the material and methods used in this study can be found in the manuscript (Chapter 3), together with the regional setting of the SFRB. Final conclusions are presented in Chapter 4.

1.2 RESEARCH AIMS

This Master's dissertation aims to contribute to the understating of the hydroclimate and vegetational dynamics in the SFRB (i.e, eastern South America) for the last ca. 45 kyr. To reach this aim, the following activities were performed:

1. Reconstruction of past changes in precipitation over the SFRB based in the δD of long-chain *n*-alkanes;
2. Reconstruction of past changes in the predominant photosynthetic pathway of SFRB vegetation based in the $\delta^{13}C$ of long-chain *n*-alkanes;
3. Reconstruction of the climatic mechanisms responsible for the inferred paleoenvironmental variations;
4. Comparison and contextualization of the obtained data with records available in the literature.

2 CHAPTER 2

2.1 LONG CHAIN *n*-ALKANES

Long-chain *n*-alkanes and other organic compounds, such as *n*-alkanoic acids, *n*-alkanols and *n*-esters, constitute the epicuticular wax, which act as a protective layer in terrestrial plants (Eglinton & Hamilton, 1967). *n*-Alkanes correspond to the group of saturated aliphatic hydrocarbons, represented by the formula C_nH_{2n+2}. Their C-C and C-H covalent bonds are exceedingly difficult to break, so these molecules tend to be preserved over geological time. These lipid biomarkers can be produced by algae, bacteria, terrestrial plants and be derived from degradation of petrogenetic processes. They are available in the form of fossils in soils and sediments from lakes, rivers and marine environments (Sachse, et al., 2012; Schefuß et al., 2003; Smith & Freeman, 2006).

The chain length can indicate the source of these compounds. Long-chain *n*-alkanes (C_{21}-C_{35}) produced by vascular terrestrial plants have a predominance of odd numbered chain, since they are compounds formed from enzymatic conversion by decarboxylation. *n*-Alkanes produced by aquatic algae and aquatic plants produce shorter chains (C_{17}-C_{21}) (Bush & McInerney, 2013; Castañeda & Schouten, 2011).

Since plants adapt to different degrees of water availability, the increase in the chain length provides a higher efficiency in retaining water, hindering evapotranspiration. Smaller odd chains (C_{17}) are characteristic of material of marine origin, such as macroalgae, phytoplankton and phanerogams (Meyers, 2003). Medium chains (C_{21}-C_{25}) are characteristic of marine macrophytes, while long chain compounds (C_{27}-C_{35}) are characteristic of terrestrial vascular plants (Bush & McInerney, 2013; Castañeda & Schouten, 2011).

Several methods have been applied to characterize the distribution of *n*-alkanes. The Carbon Preference Index (CPI) (equation 2.1) provides information about the predominance of odd over even carbon number molecular chains. Values of CPI > 1 indicate a predominance of odd chains in the sample, pointing to a possible plant source, while CPI <1 indicates that the source of the material is of petrogenic origin, or even anthropic (Eglinton & Hamilton, 1967).

$$CPI_{27\text{-}33} = 0.5 * \left(\frac{nC_{27} + nC_{29} + nC_{31} + nC_{33}}{nC_{26} + nC_{28} + nC_{30} + nC_{32}} + \frac{nC_{27} + nC_{29} + nC_{31} + nC_{33}}{nC_{28} + nC_{30} + nC_{32} + nC_{34}}\right)$$

(2.1)

Carbon fixation in photosynthesis can occur through three metabolic pathways: C3 (Calvin-Benson), C4 (Hatch-Slack) or CAM (crassulacean acid metabolism) (Bianchi & Canuel, 2011). The type of metabolism used by plants also influences the size of *n*-alkane chains. C4 plants tend to have higher concentrations of longer chain *n*-alkanes (C_{31}, C_{33}, C_{35}) than C3 plants (Garcin et al., 2014). The Average Chain Length (ACL) index (equation 2.2) is thus used to differentiate the size of the chains in *n*-alkanes.

$$ACL_{27\text{-}33} = \frac{27 * nC_{27} + 29 * nC_{29} + 31 * nC_{31} + 33 * nC_{33}}{nC_{27} + nC_{29} + nC_{31} + nC_{33}}$$

(2.2)

During photosynthesis, plants strongly fractionate carbon isotopes. Different carbon-fixing pathways produce *n*-alkanes with different carbon isotopic signatures. The C3 photosynthetic pathway presents the largest net fractionation, whereas the C4 pathway the smallest one (Diefendorf & Freimuth, 2017; O'Leary, 1988). The stable carbon isotopic composition ($\delta^{13}C$) of long-chain *n*-alkanes can be used to distinguish between plants that use the C3 (average *n*-alkane $\delta^{13}C$ of -34.7‰ for the C_{29}) or C4 photosynthetic pathways (average *n*-alkane $\delta^{13}C$ of -21.4‰ for the C_{29}) (Castañeda & Schouten, 2011).

Figure 2.1 illustrates the differences in $\delta^{13}C$ for plants using different photosynthetic metabolisms. Generally, soil bulk $\delta^{13}C$ values are more enriched than long-chain *n*-alkanes. The difference varies from biome to biome, but a study performed in South America indicates a difference of ca. 6‰ (Wu et al., 2019).

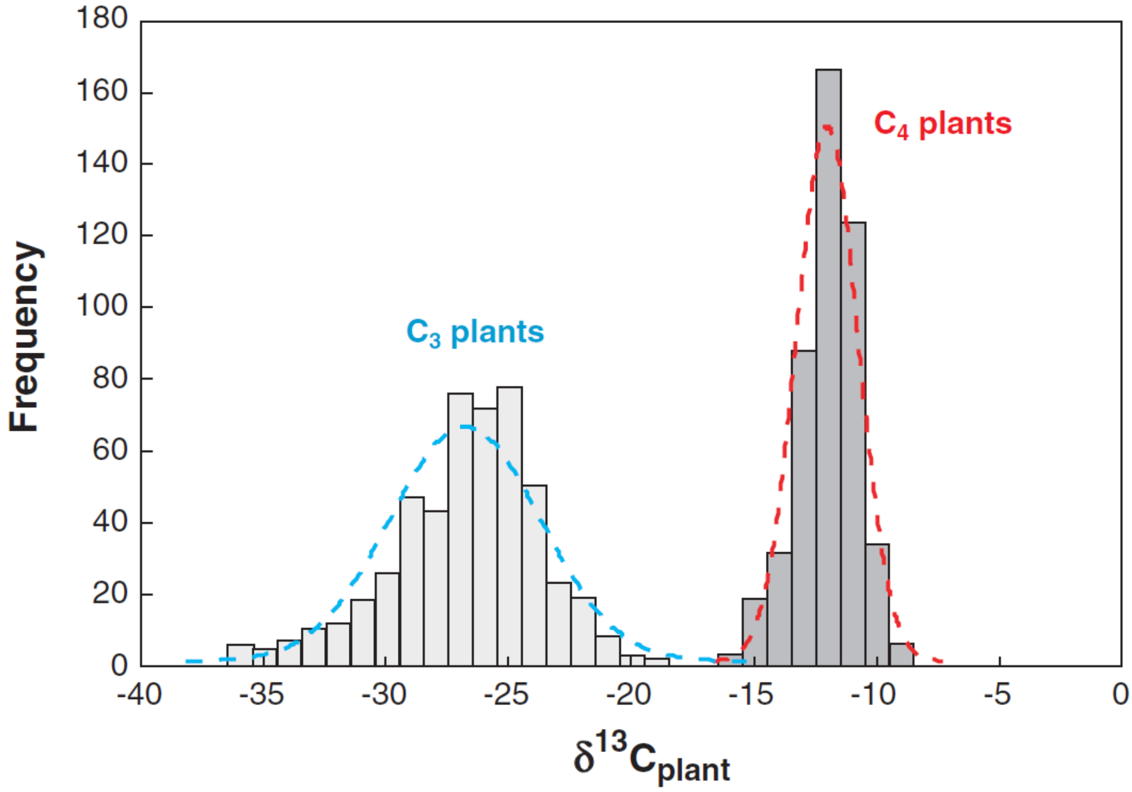

Figure 2.1 Histogram showing normal distribution of bulk C3 and C4 plant isotopic values (Tipple & Pagani, 2007).

C3 plants (trees, shrubs and cool-climate grasses) dominate Tropical forest and savannas with a closed canopy, while C4 plants (tropical grasses) dominate open savannas (Garcin et al., 2014; Lloyd et al., 2008). Thus, the analysis of long-chain *n*-alkanes $\delta^{13}C$ can provide the composition (C3 versus C4) of vegetation in tropical regions and the dominant biome (Häggi et al., 2016; Schefuß et al., 2005). Importantly, biomes do not exclusively feature C3 or C4 vegetation. Usually, they have a mix of C3 and C4 plants, as is the case of Cerrado (Toby Pennington et al., 2000).

In the absence of $\delta^{13}C$ values for modern long-chain *n*-alkanes from the different biomes of the SFRB, we compiled the $\delta^{13}C$ values available in the literature from soil bulk organic matter covering savanna (Cerrado) and forest ecosystems from the SFRB and its direct neighborhood (Figure 2.2). The compiled data confirm the more enriched $\delta^{13}C$ signal of Cerrado (median -25.4 ‰) compared to the forest signal (median -26.9 ‰).

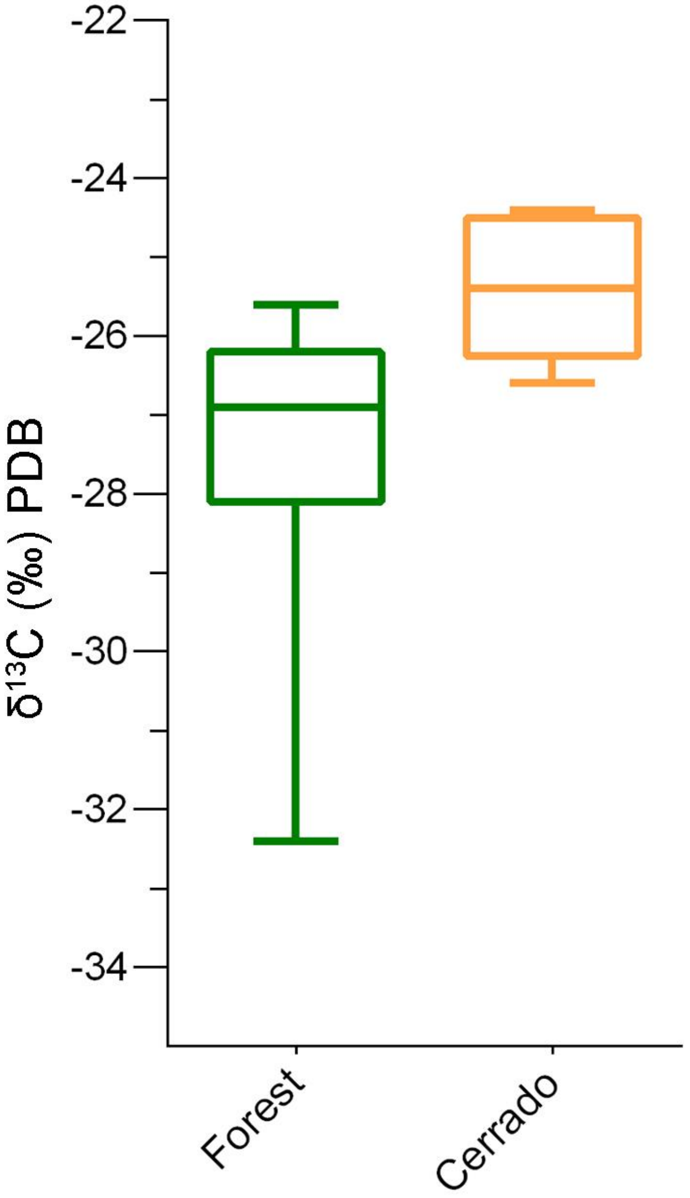

Figure 2.2 Box plots of $\delta^{13}C$ data from soil bulk organic matter available for the São Francisco River Drainage Basin and its direct neighborhood (Mendonça et al., 2010; Pessenda et al., 1996, 1998; 2010). The data for Cerrado and Forest are indicated by the orange and green box plots, respectively.

The δD of long chain *n*-alkanes indicate the environmental conditions during the formation of the epicuticular waxes. Since water is the primary source of hydrogen for photosynthetic organisms, organic hydrogen in lipids preserved in sediments deposited offshore can provide information about continental hydroclimate of a given region (Collins et al., 2017; Schefuß et al., 2005, 2011).

During sea water evaporation (δD = 0‰), the corresponding vapor will be depleted in the heavier isotope D, since $^{1}H_2{}^{16}O$ has a higher vapor pressure than $^{1}D^{16}O$. After condensation, the resulting rain is enriched in D compared to the vapor (Sachse et al., 2012).

Dansgaard (1964) identified some factors that control the δD values in precipitation: (i) "continental effect" will occur as air masses lose moisture over the continent, where the preferential loss of D results in lower δD values as air masses move further inland; (ii) "temperature effect" occurs in regions with intense temperature variability; and (iii) "amount effect", which occurs in tropical regions, where the rainfall regime is strongly marked by seasonality and, the depletion in D is related to higher precipitation rates.

The δD of long-chain *n*-alkanes reflect the isotopic composition of the water used by the producing organism (Schefuß et al., 2005) (Figure 2.3). The δD values of lipid biomarkers are offset from, but highly correlated with, the water source used by these organisms (Sachse et al., 2012). Current δD data from rainwater at SFRB stations were extracted from the Global Network of Isotopes in Precipitation (GNIP) database (Figure 2.4). δD values from the station closest to the headlands (Belo Horizonte) are more depleted than those near the northernmost station of the SFRB (Floresta), which is closest to the mouth of the river. The data confirm that within the SRFB, regions with higher amount of rainfall (Figure 1.1) show more negative δD values.

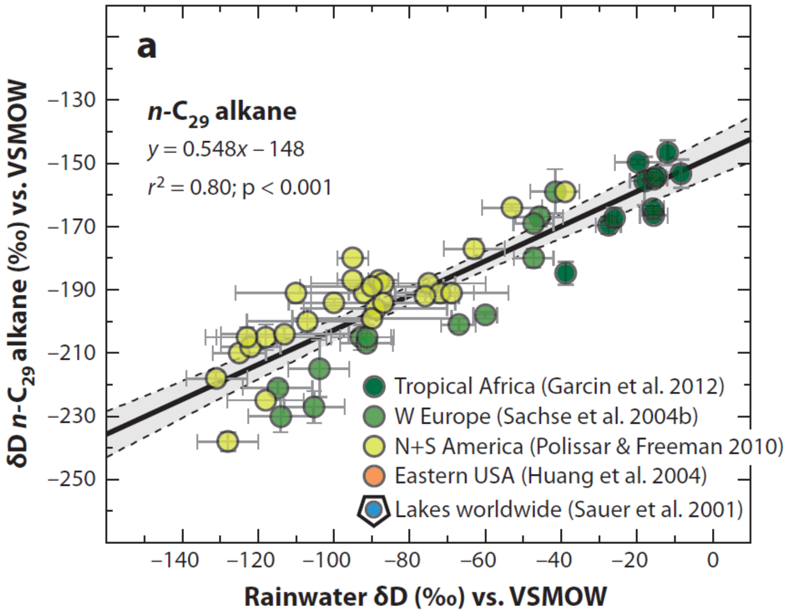

Figure 2.3 Relationships between source-water δD and lipid biomarker δD values from lake-surface sediment samples from Europe, Africa and the Americas (Sachse et al., 2012).

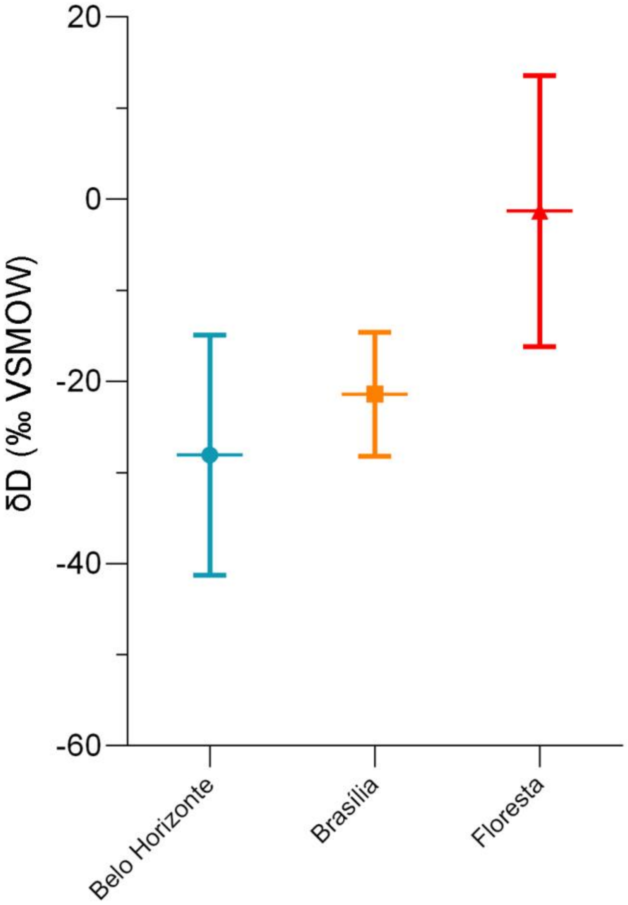

Figure 2.4. Long term means (monthly) and associated standard deviation of rainwater δD from three different stations located in direct neighborhood of the São Francisco River Drainage Basin (Global Network of Isotopes in Precipitation database, accessible at https://nucleus.iaea.org/wiser). Data from Belo Horizonte/MG (blue line and dot), Brasília/DF (orange line and square) and Floresta/PE (red line and triangle) stations.

Due to the accumulation of the lighter hydrogen isotope (^1H) in continental ice sheets during the last glacial, the mean isotopic composition of hydrogen in the rest of the global hydrological cycle became more D-enriched (by 8‰ on average) compared to present day conditions. This ice volume effect must be accounted for when reconstructing past environmental conditions by applying an ice volume correction (IVC) as the one described in equation 2.3 (Tierney and deMenocal, 2013).

$$\delta D_{wax-\mathrm{IVC}} = \frac{1000 + \delta D_{\mathrm{wax}}}{8 * 0.001 * \delta^{18}O_{\mathrm{isoice}} + 1} - 1000 \quad (2.3)$$

Where $\delta D_{\mathrm{wax-IVC}}$ represents the ice volume corrected isotope values, δD_{wax} the measured δD of plant-waxes and $\delta^{18}O_{\mathrm{isoice}}$ the effect of ice volume on the benthic $\delta^{18}O$ variation (Bintanja et al., 2005).

2.2 PALEOENVIRONMENTAL RECONSTRUCTIONS IN EASTERN SOUTH AMERICA

The SFRB is the largest hydrographic system in eastern South America. Accurate reconstructions of past vegetation in this area are critical to understand the dynamics of Neotropical biogeography and biodiversity. Despite this, the main factors that control biomes changes during the last tens of thousands of years and, at least in part, were responsible for their current distribution are still largely unknown. This is due to the small number of long paleoenvironmental reconstructions that integrate large areas of the São Francisco river basin.

Marine sedimentary records can greatly contribute to understanding past changes in continental vegetation (Häggi et al., 2017; Mulitza et al., 2017). Data from northern NE Brazil, for instance, indicated wet conditions during the YD interval that were accompanied by the expansion of Tropical forest (Bouimetarhan et al., 2018; Mulitza et al., 2017). Vegetation over northern NE Brazil also showed a response to increased precipitation during HS1, the landscape once dominated by grasses and shrubs showed an expansion in forest phytophysiognomies (Behling et al., 2000; Dupont et al., 2010; Jennerjahn et al., 2004; Mulitza et al., 2017).

These records greatly contributed to understanding the past dynamics of vegetation over northern NE Brazil. However, they are located under the influence of the Intertropical

Convergence Zone (ITCZ), a global convective belt over the oceans associated to the ascending branch of the Hadley cell and to the convergence of the NE and SE trade winds (Marshall, 2014; Schneider et al., 2014). The ITCZ annual mean latitudinal position is around 5ºN and, despite its southward displacements during HS events (Mulitza et al., 2017; Portilho-Ramos et al., 2017; Mendes et al., 2019; Venancio et al., 2020; Zhang et al., 2017), it is unlikely to have influenced the SFRB. Indeed, the northernmost portion of the SFRB is located at ca. 8ºS and does not show a typical yearly precipitation distribution for a site influenced by the southernmost position of the ITCZ (i.e., peak in precipitation during March-May) (Figure 1.1) (Garreaud et al., 2009; Hastenrath, 2012; Schneider et al., 2014).

Investigating marine sediment core M125-95-3 (Figure 1.2) (the same core investigated in this dissertation), Campos et al. (2019) suggested positive excursions in precipitation to have occurred over the SFRB during HS and the YD. The mechanism proposed to explain the positive excursions goes beyond changes in SAMS. According to Campos et al. (2019), eastern South America was affected by an anomalous tropical South Atlantic cyclonic circulation during HS and the YD. The SFRB was affected by increased precipitation mainly during the extended austral summer. In the continent, speleothem records (Stríkis et al., 2018) indeed indicate increases in precipitation during HS and the YD. Importantly, neither the marine sediment core nor the speleothems show orbital signals, neither precession nor obliquity.

Several palynological studies have been carried out based on paleoenvironmental archives collected within or in the direct neighborhood of the SFRB (Table 2.1; Figure 2.5). Horák-Terra et al. (2020) suggest the occurrence of a long dry season from ca. 35-25 ka BP in the eastern edge of the basin (Figure 2.5), with a reduction in arboreal pollen (AP) (Figure 2.6f) and the highest δ^{13}C values (Figure 2.6c), indicating a higher contribution of C4 plants during this period than in any other from this record. Cassino et al (2020) indicate the occurrence of an open landscape in central Cerrado (Figure 2.5) at ca. 19-13 ka BP followed by a forest/arboreal savanna expansion between ca. 12.5 and 11.2 ka BP (Figure 2.6e). Humid conditions associated with the expansion of trees and a short dry season were indicated for Chapadão dos Gerais (Figure 2.5) (Cassino & Meyer, 2013) between ca. 13.5 and 11.6 ka BP, and for Salitre de Minas (Figure 2.5) (Ledru, 1993) between ca. 13 and 11 ka BP. Northern Cerrado data (Cassino et al., 2018) also indicate an increase in AP during the Pleistocene-Holocene transition (ca. 14.6, 13.4, 12.2 and 11 ka BP samples). During the early Holocene, the southern portion of the SFRB showed an open landscape with small areas of gallery forests along the drainage systems (Behling, 2003), associated with a moisture decline

(Cassino et al., 2020). On the other hand, in the northern portion of the SFRB (currently dominated by Caatinga, Figure 2.5) the early Holocene was characterized by the presence of a dense forest cover with a high frequency of tree elements from the Atlantic Forest (De Oliveira et al., 1999).

Despite the detailed descriptions about variations of the phytophysiognomies, none of these studies cover one complete obliquity period (ca. 41 ka) (Table 2.1), which could facilitate the identification of a possible obliquity influence on vegetation. In addition, the different hydroclimate controls active over distinct portions of the SFRB (Figure 1.1) make any specific continental paleoenvironmental record unable to register the basin-integrated vegetational dynamics. Indeed, past variations in austral summer insolation, for instance, resulted in opposite hydroclimate changes in the southern versus the northern portions of the SFRB (Prado et al., 2013; Prado et al., 2013b). Thus, only a paleoenvironmental archive that to some extent integrates a larger portion of the SFRB would be able to record orbital-scale changes in the vegetation of the basin.

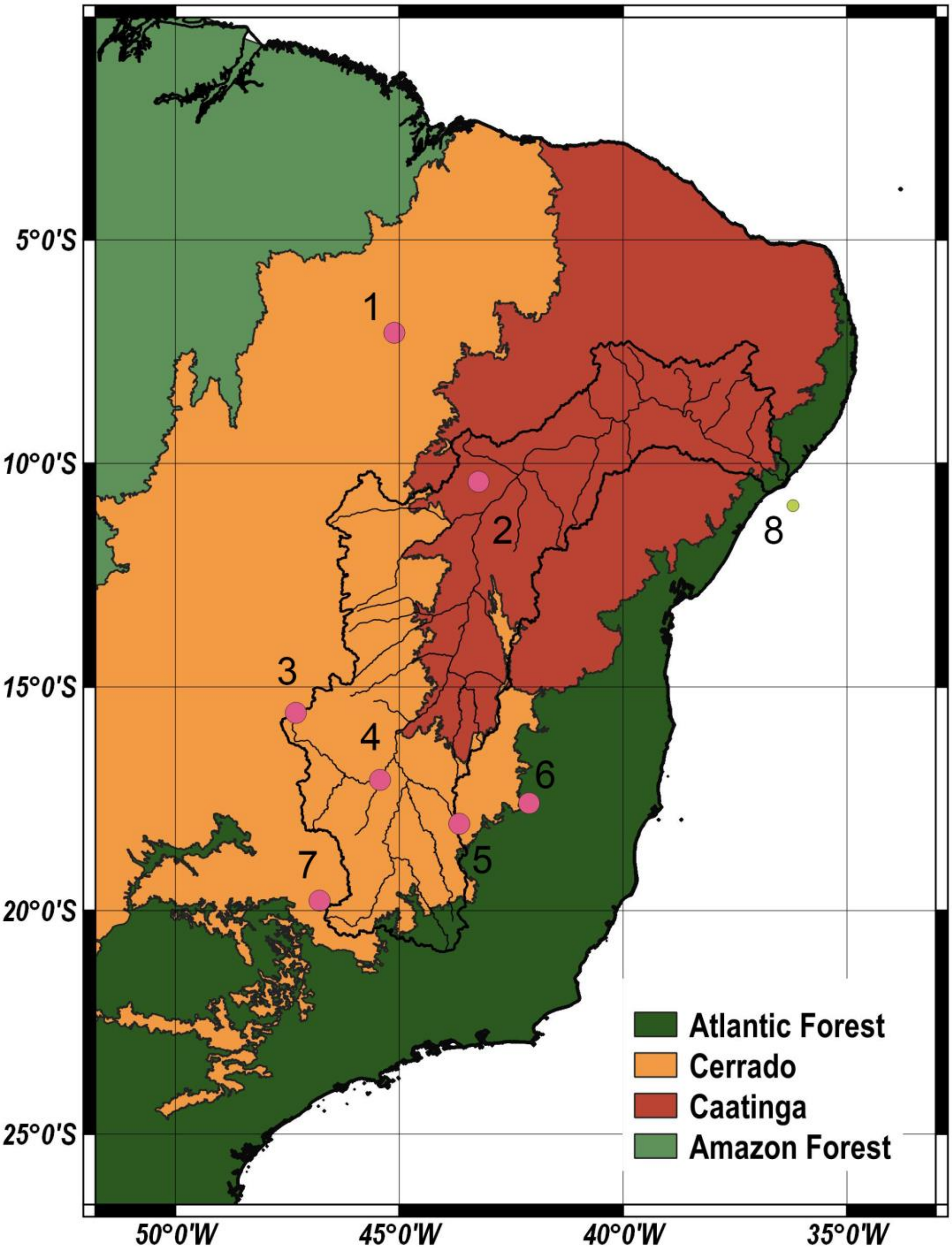

Figure 2.5 Location of selected palynological records (pink circles) from the São Francisco River Drainage Basin and its direct neighborhood, on top of the distribution of Brazilian biomes (IBGE, 2004). **1.** São José palm swamp (Cassino et al., 2018) **2.** Icatu River Valley (De Oliveira et al., 1999a) **3.** Lagoa Feia (Cassino et al., 2020) **4.** Chapadão dos Gerais (Franco Cassino & Meyer, 2013) **5.** Pinheiro mire (Horák-Terra et al., 2020) **6.** Lagoa Nova (Behling, 2003) **7.** Salitre de Minas (Ledru, 1993). The location of the M125-95-3 marine core is indicated by the green circle in **8**.

Table 2.1 Selected palynological records from the São Francisco River Drainage Basin and its direct neighborhood. For the location of the records see Figure 2.5.

Location	Number of the record in Figure 2.5	Type of record	Interval covered by the record (ka BP)	Reference
Pinheiro Mire	5	Peat core	35-0	Horák-Terra et al. (2020)
Lagoa Feia	3	Lake core	19-4.5	Cassino et al. (2020)
São José palm swamp	1	Peat core	15.7-0	Cassino et al. (2018)
Icatu river valley	2	Peat core	10.9-4.2	Oliveira et al. (1999)
Salitre de Minas	7	Peat core	32-3.1	Ledru (1993)
Lagoa Nova	6	Lake core	10.2-0.2	Behling (2003)
Vereda Laçador	4	Palm swamp	13.3-1.3	Cassino & Meyer (2013)

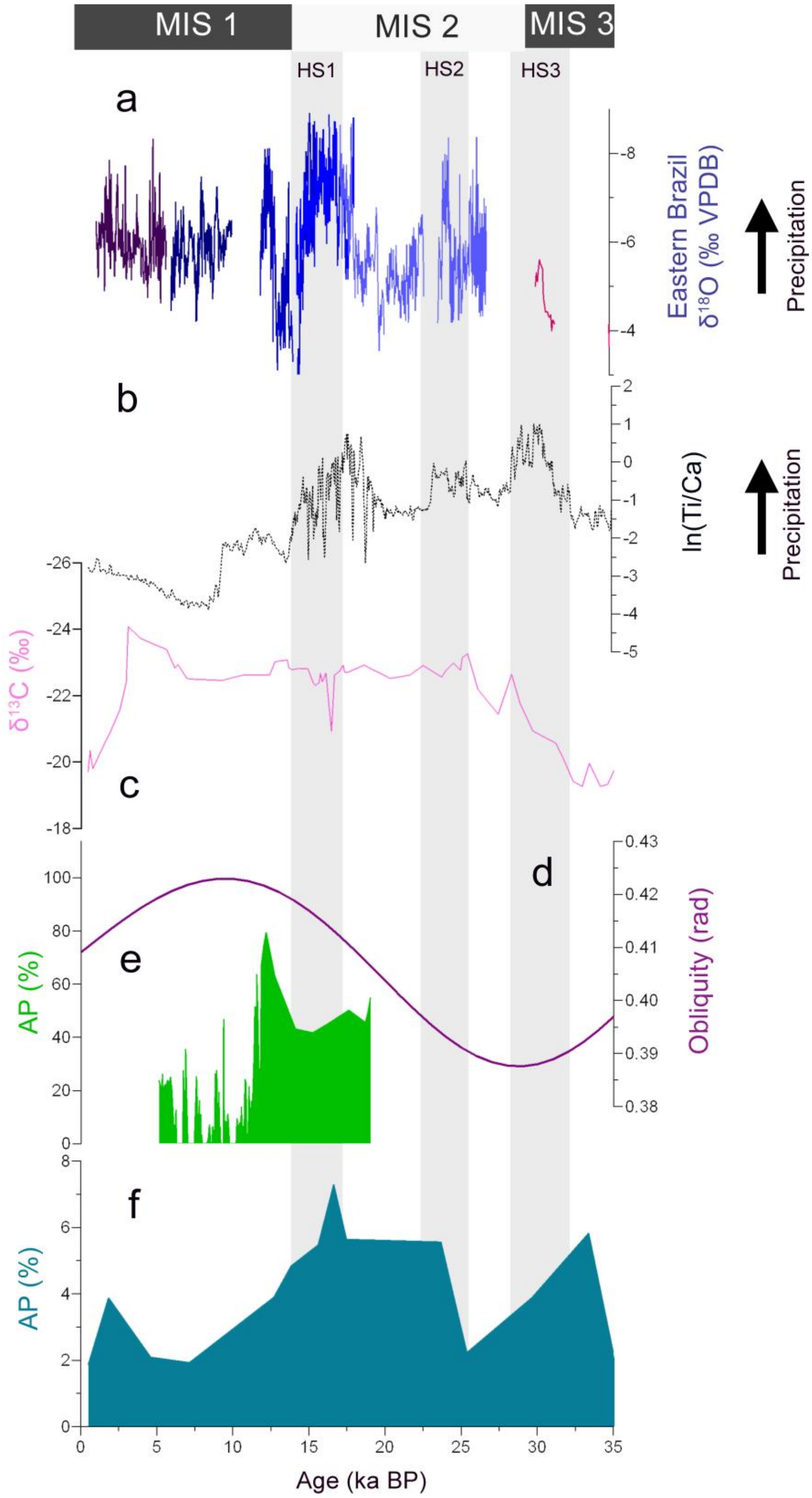

Figure 2.6 Eastern South American paleoenvironmental records over the last ca. 35 kyr. **A.** Speleothems stable oxygen isotopic record ($\delta^{18}O$) from eastern Brazil (Stríkis et al., 2018). **B.** ln(Ti/Ca) data of core M125-95-3 (Campos et al., 2019). **C.** $\delta^{13}C$ from peat core Pinheiro mire (Horák-Terra et al., 2020). **D.** Obliquity values (Laskar et al., 2004). **E.** Arboreal pollen percentage (AP %) from Lagoa Feia (Cassino et al., 2020). **F.** AP% from Pinheiro mire (Horák-Terra et al., 2020). See Table 2.1 and Figure 2.5 for the location of the described records.

3 CHAPTER 3

Changes in obliquity drive biome shifts in eastern tropical South America

Ferreira, Jaqueline Q.[a,b]; Chiessi, Cristiano M.[a]; Hirota, Marina[c]; Oliveira, Rafael S.[d]; Prange, Matthias[e]; Häggi, Christoph[f];. Crivellari, Stefano[a]; Bertassoli, Dailson J[a]; Campos, Marília C[b]; Mulitza, Stefan[e]; Albuquerque, Ana Luiza S.[g]; Bahr, André[h]; Schefuß, Enno[e]

[a]School of Arts, Sciences and Humanities, University of São Paulo, São Paulo, Brazil

[b]Institute of Geosciences, University of São Paulo, São Paulo, Brazil

[c]Department of Physics, Federal University of Santa Catarina, Florianópolis, Brazil

[d]Department of Plant Biology, University of Campinas, Campinas, Brazil

[e]MARUM – Center for Marine Environmental Sciences, University of Bremen, Bremen, Germany

[f]Department of Earth Sciences, University of Southern California, Los Angeles, USA

[g]Gradutate Program on Geosciences (Geochemistry), Fluminense Federal University, Niterói, Brazil

[h]Institute of Earth Sciences, Heidelberg University, Heidelberg, Germany

Keywords: Quaternary; South America; vegetation; orbital forcing; long chain *n*-alkanes; precipitation

3.1 ABSTRACT

Despite its great ecological importance, the main factors governing tree density in tropical savannas as well as the savanna-forest boundaries are still largely unknown. Here we address this issue, showing records of long-chain *n*-alkanes stable carbon ($\delta^{13}C$) and hydrogen (δD) isotopes spanning the last ca. 45 kyr from a marine sediment core collected off eastern tropical South America. While $\delta^{13}C$ is a proxy for the main photosynthetic pathway of continental vegetation tracking the relative proportion of C3 (mainly trees) versus C4 (mainly grasses) plants, δD is a proxy for continental precipitation tracking the amount of rainfall. The investigated core was collected off the mouth of the São Francisco river drainage basin, a tropical savanna-dominated region with dry austral winter. On top of millennial-scale changes, we identify for the first time a marked obliquity control over the expansion and

contraction of tree and grass dominated biomes. During periods of maximum (minimum) obliquity, trees (grasses) reached maximum coverage. Importantly, our δD records do not indicate orbital-scale changes in precipitation. We suggest that maximum (minimum) obliquity decreased (increased) the length of the dry season allowing (hampering) the expansion of tree dominated vegetation. Periods of maximum (minimum) obliquity increased (decreased) the intra-hemispheric insolation gradient during austral winter, strengthening the austral Hadley circulation and the southeastern trade winds. Both processes slightly increased winter precipitation over the São Francisco river drainage basin, decreasing the length of the dry season. Our results suggest that the dry season length is a governing factor in the long-term control of tree density in tropical savannas.

3.2 INTRODUCTION

Savannas can be defined as tree-grass systems, with discontinuous woody cover and a continuous grass layer (House et al., 2003; Ratnam et al., 2011; Sankaran et al., 2004). These biomes are present in a wide range of climate conditions (House et al., 2003; Scholes & Archer, 1997) and have enormous socioeconomic relevance since they cover substantial areas and act as biodiversity hotspots (Myers et al., 2000). Tree cover density is highly variable in different savanna types, and several factors like the availability of nutrients and water, as well the action of fire and herbivores may influence this parameter (Bond, 2005, 2008; Bond & Keeley, 2005; Staver et al., 2011b). However, the main factors that govern the dynamics of tree-grass interactions in tropical savannas are still largely unknown (Hoffmann et al., 2012a; House et al., 2003; Lloyd et al., 2008; Sankaran et al., 2004).

The extension of tree cover has a profound ecological importance for savannas. For instance, with the increase of tress, grass production usually declines (Scholes & Archer, 1997). The closed canopy reduces the flammability of the ecosystem, directly reducing fire spread (Hennenberg et al., 2006; Hoffmann et al., 2012a; Hoffmann et al., 2012b). In addition, tree cover density in savannas also intensely impacts herbivore communities (Riginos & Grace, 2008), as well as the carbon and hydrological cycles (Grace et al., 2006; Jackson et al., 2002; Simioni et al., 2003).

Heavily wooded savannas are structurally similar to forests (Ratnam et al., 2011). These two biomes have been characterized as alternative stable states (Hirota et al., 2010, 2011; Staver et al., 2011a, 2011b). In addition, ecological models that are used to predict the savanna to tropical forest transition fall short in mimicking the entire complexity of natural regimes and are not fully able to capture long-term impacts (Pausas & Bond, 2020). Paleoenvironmental records can substantially contribute for a better understanding of this issue.

Here we assess the response of savannas from eastern tropical South America to hydroclimate changes during the last ca. 45 kyr. Therefore, we analyzed a marine sediment core that archived sediments from the São Francisco River Drainage Basin (SFRB), the largest basin in eastern tropical South America (Figure 3.1). We used the stable carbon ($\delta^{13}C$) and hydrogen (δD) isotopic composition of epicuticular waxes (i.e., long-chain *n*-alkanes) of terrestrial higher plants to reconstruct the main photosynthetic pathway of vegetation (i.e., C3 trees versus C4 grasses) and the amount of precipitation, respectively. Our findings unambiguously show enhanced tree cover during periods of decreased dry season length (DSL). In addition, we show that subtle changes in modern DSL is a governing factor over tree density in the SFRB.

3.3 REGIONAL SETTING

The SFRB (ca. 7-21ºS and 48-35ºW) is the largest river basin in eastern South America (Figure 3.1) with annual mean water discharge of 2846 m^3/s (ANA, 2015). Precipitation in the southern portion of the SFRB mainly occurs during austral summer (December-February), when the moisture transported by the NE trade winds allows the development of the South American Monsoon System (SAMS) (Marengo 2001; Vera et al. 2006). The main convective activity of the SAMS is placed over western Brazil and extends in a NW-SE elongated convective belt over southeastern South America and the adjacent western South Atlantic (Carvalho et al., 2004). This feature is known as the South Atlantic Convergence Zone (SACZ). In the southern portion of the SFRB mean annual precipitation reaches 2000 mm/yr and the dry season length (i.e., the number of months with mean precipitation lower than 100 mm/month) is 6-7 months long. In the upper troposphere, the convective activity associated to the SAMS produces the Bolivian High over the Altiplano that is dynamically linked to the Nordeste Low over northeastern Brazil (Lenters & Cook, 1997). The Nordeste Low, in turn, produces large-scale subsidence over northeastern Brazil that affects the northern portion of the SFRB, where mean annual precipitation is lower than 500 mm/yr and the dry season length is ca. 11 months-long. Between these two portions, the central SFRB shows mean annual precipitation of ca. 1200 mm/yr and dry season length of 6-10 months. Over a narrow stripe along the coast of northeastern Brazil, rainfall maximum occurs during austral autumn and winter and is associated to breeze circulation (Kousky, 1979), as well to the occurrence of easterly wave disturbances in the wind field (Torres & Ferreira, 2011), which locally increase low-level convergence and rainfall (Gomes et al., 2015; Torres & Ferreira, 2011). This feature affects the mouth of the SFRB.

Atlantic Forest occurs over the southern portion of the SFRB and along a narrow coastal stripe along the coast of northeastern Brazil (Figure 3.1), covering ca. 5% of the SFRB (Souza et al., 2020). This biome is composed of two major vegetation types: the Atlantic Rain Forest, which runs along the coastline, and the Atlantic Semi-deciduous Forest, which occupies higher elevation inland areas (Oliveira-Filho & Fontes, 2000). The northern portion of the SFRB is covered by Caatinga (ca. 49% of the SFRB), a type of tropical dry forest and shrubland, composed by xerophytic, woody, thorny and deciduous physiognomies (Sampaio, 1995). Between these extreme biomes, tropical savanna, the Cerrado, occupy a vast central portion of the SFRB (ca. 45% of the SFRB). The Cerrado is a complex ecosystem with mixed trees and grasses, ranging from tree-less open vegetation (Campo Limpo) with a dense grassland ground and small shrubs, to a closed canopy with a dense occurrence of trees (Cerradão) and associated gallery forests following the watercourses (Bridgewater et al., 2004; Da Silva & Bates, 2002; Toby Pennington et al., 2000). The dry forest and savanna open habitats act as a corridor splitting the Atlantic Forest (SE) and the Amazonian Forest (NE) (Azevedo et al., 2020).

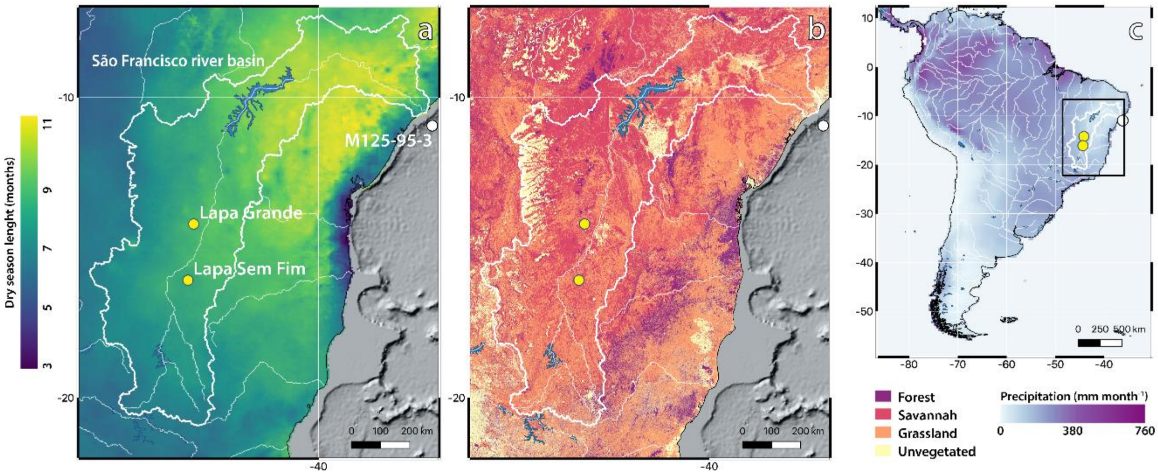

Figure 3.1 Climatological and ecological features of the São Francisco River Basin and adjacent areas. **A.** Dry season length (Funk et al., 2015) **B.** Distribution of tropical forest, savanna and grassland based on Mapbiomas land cover data (Souza et al., 2020) **C.** Mean annual precipitation (Harris et al., 2020). The black rectangle in C depicts the area shown in A and B. The location of marine sediment core M125-95-3 is indicated by a white circle. The location of the Lapa Grande and Lapa Sem Fim speleothem records are indicated by yellow circles in all subplots (Stríkis et al., 2018).

3.4 MATERIAL AND METHODS

3.4.1 Marine sediment core and geoinformation

We investigated marine sediment core M125-95-3 (10.94º S, 36.20º W, 1897 m water depth, 10.4 m core length) collected off the São Francisco river mouth in the eastern South American continental slope (Figure 3.1) during RV Meteor cruise M125 (Bahr et al., 2016).

For the geostatistical analyses the following geographic information were used: (i) mean annual precipitation and DSL calculated from monthly Climate Hazard group Infrared Precipitation with Stations (CHIRPS) precipitation data covering the 1981-2017 period (Funk et al., 2015); and (ii) distribution of biomes (i.e., forest, savanna, grassland) and land use data from MapBiomas (Souza et al., 2020).

3.4.2 Age model

Nine calibrated ^{14}C accelerator mass spectrometry ages performed on planktonic foraminifera and three benthic foraminifera oxygen isotopic composition tie-points were used to produce the age model of core M125-95-3. Absolute ^{14}C ages were calibrated with the IntCal13 calibration curve (Reimer et al., 2013) with a variable simulated reservoir age from the transient modeling experiments described in Butzin et al. (2017). The benthic foraminifera oxygen isotopic reference curve from Govin et al. (2014) was used to establish the tie-points. The age modeling algorithm BACON v. 2.2 (Blaauw & Christeny, 2011) was used within the software PaleoDataView v. 0.8.3.4 (Langner & Mulitza, n.d.) to perform the age model. The investigated section of core M125-95-3 (i.e., uppermost 470 cm) covers the last ca. 45 kyr and shows an average sedimentation rate of 10.4 cm/kyr. Further details regarding the age model are provided in Campos et al. (2019).

3.4.3 Lipids extraction and compound isolation

Freeze-dried (Christ Beta 1-8 LDplus) sediment samples (ca. 6 g) were ground with an agate pestle and mortar. A squalene internal standard was added to the samples before extraction. Lipid compounds were extracted with a DIONEX Accelerated Solvent Extractor (ASE200) at 100^{o}C and 1000 psi using a dichloromethane methanol (DCM:MeOH 9:1 v/v) solution, in three cycles of five min each. The solvent was removed by rotary evaporation (Heidolph ROTOVAP system) to near dryness and elemental sulfur was removed from the extracts using copper turnings. Lipid extracts were saponified using 0.1M potassium hydroxide (K0H) in a MeOH solution at 85°C for 2 h and the neutral fraction was extracted in a deactivated silica (1% H_2O) column. The column was eluted with hexane, DCM and DCM:MeOH (1:1), yielding the *n*-alkane, ketone and polar fractions. The *n*-alkane fraction was cleaned by elution over 4 cm of $AgNO_3$-coated silica.

3.4.4 n-Alkane quantification

The *n*-alkane fraction was analyzed in a Thermo Fisher Scientific Focus gas chromatograph (GC) equipped with an Rxi5 ms 30 x column (30 m, 0.25 mm, 0.25 mm) and a flame ionization detector (FID). To quantify the *n*-alkane concentrations, the resulting peak areas were manually integrated and compared with an external standard, that was run every six samples. Precision of compound quantification is about 5% based on multiple standard analyses. We calculate the average chain length (ACL) and the carbon preference index (CPI) following equations (3.1) and (3.2), respectively:

$$ACL_{25\text{-}33} = \frac{27 * nC_{27} + 29 * nC_{29} + 31 * nC_{31} + 33 * nC_{33}}{nC_{27} + nC_{29} + nC_{31} + nC_{33}} \tag{3.1}$$

$$CPI_{25\text{-}33} = 0.5 * \left(\frac{nC_{27} + nC_{29} + nC_{31} + nC_{33}}{nC_{26} + nC_{28} + nC_{30} + nC_{32}} + \frac{nC_{27} + nC_{29} + nC_{31} + nC_{33}}{nC_{28} + nC_{30} + nC_{32} + nC_{34}}\right) \tag{3.2}$$

3.4.5 Compound-specific isotope analyses

Compound-specific hydrogen δD analyses (C_{29} and C_{31} *n*-alkanes) were carried out by gas chromatography-isotope ratio mass spectrometry (GC-IRMS) with a Thermo Fisher Scientific MAT 253 coupled via a GC Isolink operated at 1420°C to a Thermo Fisher Scientific Trace GC. δD compositions were measured against a calibrated H_2 reference gas. Isotope values are reported in ‰ versus Vienna Standard Mean Ocean Water (VSMOW).

Compound-specific $\delta^{13}C$ analyses (C_{29} and C_{31} *n*-alkanes) were performed by GC-IRMS on a Thermo Fisher MAT 252 coupled via a GCC combustion interface with a nickel catalyzer operated at 1000°C to a Thermo Fisher Scientific Trace GC. $\delta^{13}C$ compositions were measured against a calibrated CO_2 reference gas. Isotope values are reported in ‰ versus Vienna Pee Dee Belemnite (VPDB).

3.4.6 Ice volume correction

Global mean seawater was isotopically heavier during the last glacial compared to the present interglacial due to the larger ice volume (Schrag et al., 2002). We removed the effect of changing ice volume on the isotopic composition of δD using the following equation 3.3 (Tierney & DeMenocal, 2013):

$$\delta D_{wax-\mathrm{IVC}} = \frac{1000 + \delta D_{\mathrm{wax}}}{8 * 0.001 * \delta^{18}O_{\mathrm{isoice}} + 1} - 1000 \tag{3.3}$$

where $\delta D_{\mathrm{wax-IVC}}$ is the ice volume corrected isotope values, δD_{wax} is the measured plant-wax values and $\delta^{18}O_{\mathrm{isoice}}$ is the effect of ice volume on the benthic $\delta^{18}O$ variation according to Bintanja et al. (2005).

3.4.7 Geoinformation processing

We used MapBiomas database (spatial resolution 30m x 30m) to extract the current occurrence of tropical forest, savanna and grasslands in the area 7-22°S, 48-36°W that encompasses the SFRB (Figure 3.1) (Souza et al., 2020). We chose to analyze an area that is slightly larger than the SFRB in order to have a more representative area covered by tropical forests, since this biome currently covers a reduced area of the basin (Figure 3.1). Because MapBiomas allows the identification and exclusion of areas with strong human-driven change, we were able to filter out the intense human interference in the SFRB. In addition, given that savannas also comprise more open landscapes, hereafter savannas include both the savanna and grasslands classes from MapBiomas.

Mean monthly precipitation values were extracted from the CHIRPS database (Funk et al., 2015), and refer to mean values for the interval 1981-2017. We selected data for the same box that extends the original SFRB area (7-22°S, 48-36°W). We filtered out areas with mean annual precipitation < 1,000 mm/yr, since the bi-stability range of forests and savannas in the neotropics was characterized to occur between 1,000 and 2,500 mm (Staver et al., 2011b). DSL is defined as the number of months with precipitation < 100 mm/month.

3.5 RESULTS

Long-chain *n*-alkanes $ACL_{25\text{-}33}$ values in core M125-95-3 range from 28.6 to 30.7 (average 30.2) (Supplementary Figure S1). $CPI_{27\text{-}33}$ values range from 1.1 to 4.5 (average 3.2). The δD_{29} values vary between -163.7 and -124.5 ‰ (average -145.5 ± 1.9 ‰), and the δD_{31} values vary between -164.9 and -118.0 ‰ (average -152.2 ± 2.1 ‰) (Figure 3.2). Both datasets (i.e., δD_{29} and δD_{31}) show similar changes with an average offset of 6.3 ± 2.5 ‰ (i.e., δD_{29} values are systematically higher than δD_{31} values) from the base of the record until ca. 12.5 ka BP. During the Holocene, the δD_{29} values do not show major changes while the δD_{31} values show a multi-millennial increasing trend. δD_{wax} (i.e., average of δD_{29} and δD_{31} values) shows an average of -150.7 ± 2.0 ‰ during the last glacial and -136.3 ±2.0 ‰ during the Holocene (Figure 3.3). The δD_{wax} record does not show a clear orbital trend, but shows substantial millennial-scale negative excursions, that coincide with HS4 (amplitude of -15.6 ‰), HS3 (amplitude of -11.7 ‰), HS2 (amplitude of -15.3 ‰) and HS1 (amplitude of -29.2 ‰). The millennial-scale negative excursions are present in both δD_{29} and δD_{31} records.

The $\delta^{13}C_{29}$ values range from -31.1 to -28.9 ‰ (average -30.1 ± 0.2 ‰), and the $\delta^{13}C_{31}$ ranges from -30.1 to -26.9 ‰ (average -28.6 ± 0.2 ‰) (Figure 3.2). Both datasets (i.e., $\delta^{13}C_{29}$ and $\delta^{13}C_{31}$) show similar changes with an average offset of 1.4 ± 0.3 ‰ (i.e., $\delta^{13}C_{29}$ values are systematically lower than $\delta^{13}C_{31}$ values) throughout the investigated section of core M125-95-3. $\delta^{13}C_{wax}$ (i.e., average of δC_{29} and δC_{31} values) shows an average of -29.4 ± 0.2 ‰ (Figure 3.3). The record shows an orbital-scale quasi-sinusoidal trend, with most enriched values of -27.9 ± 0.2 ‰ at ca. 29.0 ka BP, and most depleted values of -30.5 ±0.2 ‰ at ca. 15.0 ka BP.

The modern median DSL of the region covered by savanna in the area 7-22°S, 48-36°W that encompasses the SFRB is 7.4 ± 0.4 (n=3535) months and the modern median DSL of the region covered by tropical forest is 7.0 ± 0.5 (n=855) months (Figure 3.4). The Kruskal Wallis test indicates that the difference between the savanna and tropical forest median DSL values is significant.

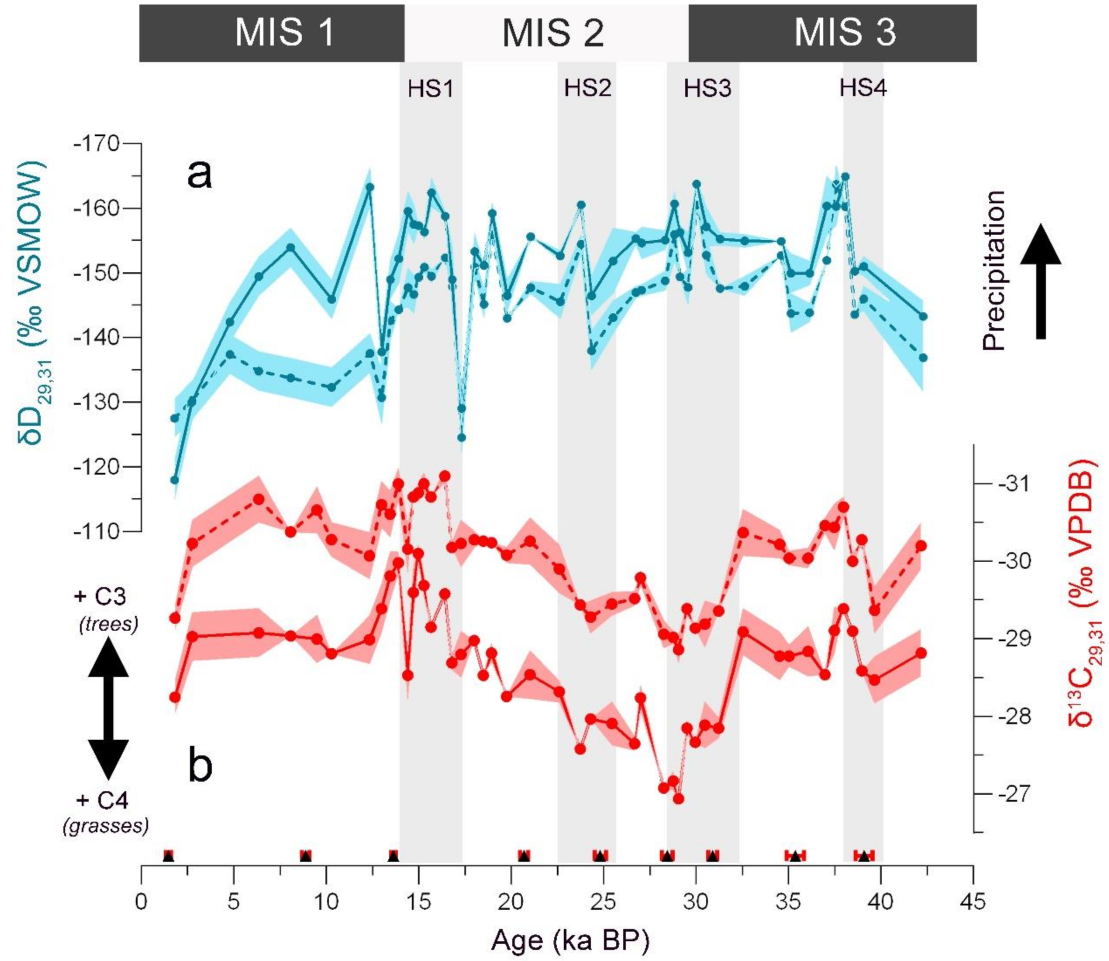

Figure 3.2 Stable hydrogen (δD) and carbon ($\delta^{13}C$) isotopic records of plant waxes from marine sediment core M125-95-3 for the last ca. 45 kyr. **A**. Ice volume corrected δD_{29} (dashed line) and δD_{31} (continuous line) values recording changes in precipitation over the São Francisco River Drainage Basin (SFRB). **B.** $\delta^{13}C_{29}$ (dashed line) and $\delta^{13}C_{31}$ (continuous line) values recording changes in the relative abundance of C3 versus C4 vegetation in the SFRB. Calibrated ^{14}C accelerator mass spectrometry ages with 2 sigma error of core M125-95-3 are indicated by triangles on the lower axis. The grey bars indicate Heinrich Stadials (HS) 4 to 1. Marine Isotope Stages (MIS) are depicted on top of panel A. Shaded areas in the isotope records indicate the standard deviation of isotope values based on standard measurements.

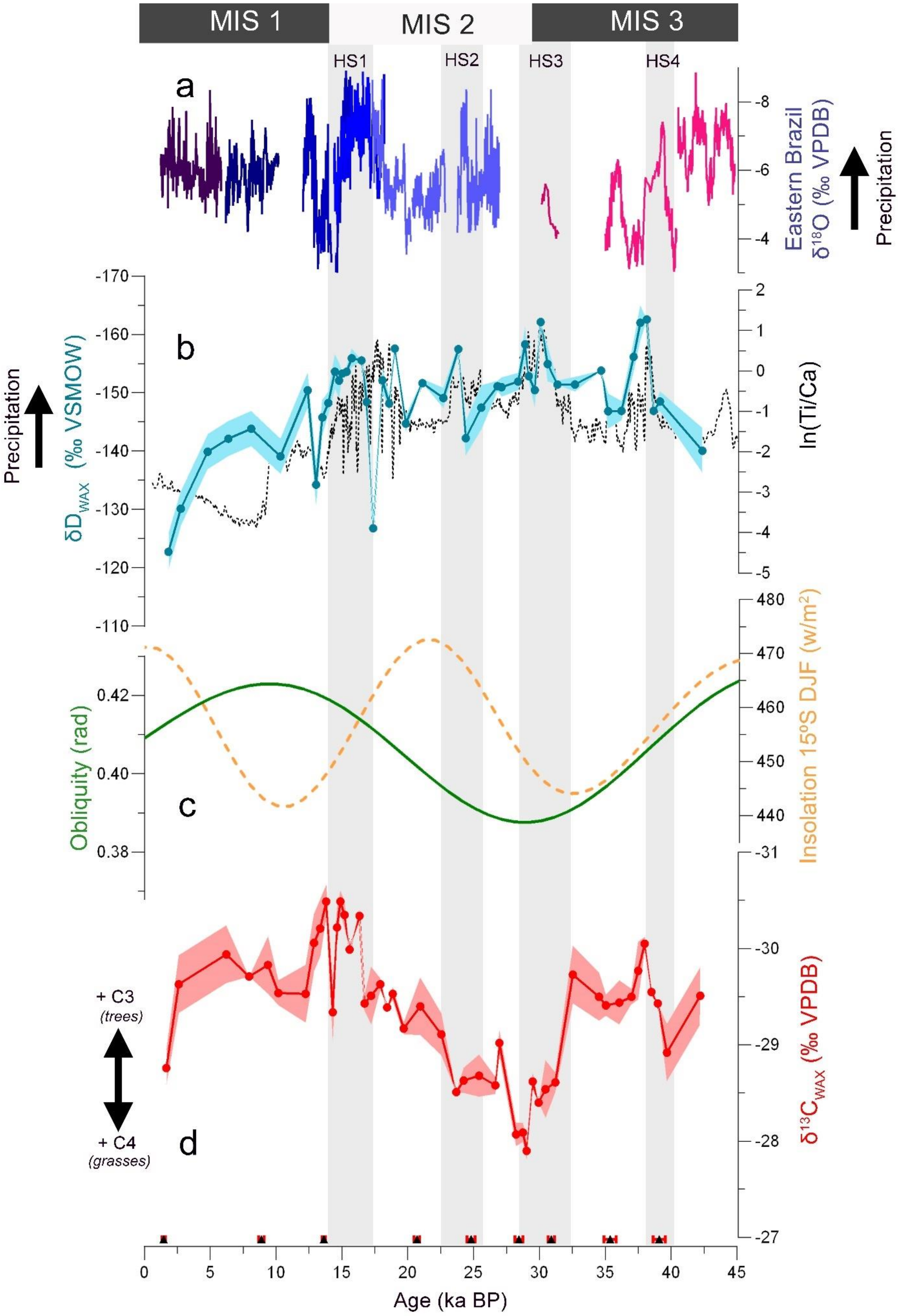

Figure 3.3 Precipitation and vegetation reconstructions for the São Francisco River Drainage Basin for the last ca. 45 kyr. **A**. Speleothem stable oxygen isotopic record ($\delta^{18}O$) from eastern Brazil (Stríkis et al., 2018). **B**. Plant

waxes stable hydrogen isotopic record (δD_{wax}) of marine sediment core M125-95-3 representing average values between C_{29} and C_{31} *n*-alkanes (blue continuous line) (this study); ln(Ti/Ca) data of core M125-95-3 (dotted black line) (Campos et al., 2019). **C**. Austral summer (December-February) insolation values for 15ºS (Laskar et al., 2004); obliquity values (Laskar et al., 2004). **D.** Plant waxes stable carbon isotopic record ($\delta^{13}C_{wax}$) of core M125-95-3 representing average values between C_{29} and C_{31} *n*-alkanes. Calibrated ^{14}C accelerator mass spectrometry ages with 2 sigma error of core M125-95-3 are indicated by triangles on the lower axis. The grey bar indicates the Heinrich Stadial (HS) 4 to 1. Marine Isotope Stages (MIS) are depicted on top of the panel A. Shaded areas in the isotope records indicate the standard deviation of isotope values.

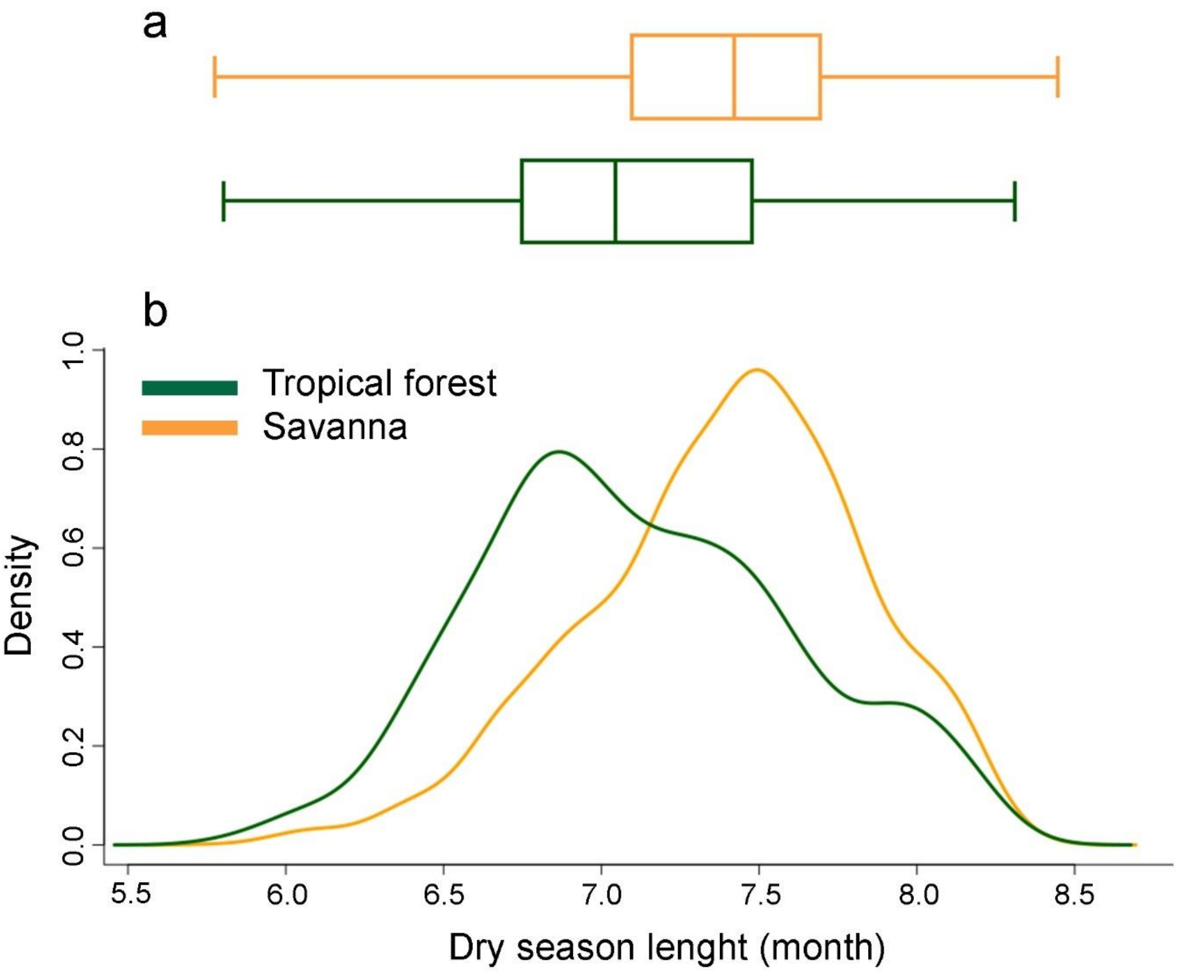

Figure 3.4 Distribution of the dry season length (DSL) (Funk et al., 2015) in tropical forest and savanna (i.e., savanna plus grasslands) domains (Souza et al., 2020) over eastern tropical South America (i.e., 7-22ºS, 48-36ºW), encompassing the São Francisco river drainage basin. **A.** Box plots of the DSL for tropical forest and savanna (i.e., savanna plus grasslands). **B.** Density plots of the DSL.

3.6 DISCUSSION

3.6.1 Orbital forcing

Despite the strong control that precession exerts over the strength of the SAMS (e.g., Cheng et al. 2013b; Cruz et al. 2005; Hou et al. 2020) neither our δD_{wax} nor our $\delta^{13}C_{wax}$ records show this type of orbital pacing (Figure 3.3). We suggest that the lack of a precession signal is due to the location of the SFRB. Over lowland tropical South America, changes in the strength of the SAMS related to precession produce a precipitation antiphase between northeastern Brazil and the rest of lowland tropical South America (Fig. 3.1c) (Cruz et al., 2009; Prado et al., 2013a). At the transition between these two domains, the integrated signal of the SFRB (as captured by our isotopic records) does not show a precession pacing (Figure 3.3). When the southern portion of the basin is influenced by a strong SAMS (i.e., high austral summer insolation), its northern portion experiences deficit in precipitation, and vice-versa. Indeed, speleothem-based hydroclimate records from the central SFRB (Stríkis et al., 2011, 2018) as well as the ln(Ti/Ca) record from marine core M125-95-3 that integrates the whole SFRB (Campos et al., 2019) do not show a clear precession signal either, agreeing with our δD_{wax} record (Figure 3.3a, b).

While our δD_{wax} record shows no orbital signal at all, our $\delta^{13}C_{wax}$ record shows a prominent obliquity pacing (Figure 3.3d). To our knowledge, an obliquity pacing has not been reported in paleoenvironmental records from lowland tropical South America. Under maximum obliquity, the mean annual meridional insolation gradient decreases (Huybers, 2006), with positive anomalies in the annual average insolation (ca. 16 W/m^2) occurring at high latitudes (ca. 80^o), no net insolation change at ca. 40^o, and negative anomalies (ca. 4 W/m^2) in the equator (Bosmans et al., 2015). Seasonally, however, negative (positive) insolation anomalies occur in the mid to low (high to mid) latitudes of the winter (summer) hemisphere. Importantly, in the winter hemisphere, maximum decrease in insolation occurs at ca. 40^o, and reaches up to 15 W/m^2 (Huybers, 2007). These changes in the seasonal distribution of insolation result, for example, in a stronger mid- to low latitude insolation gradient in the winter hemisphere (Mantsis et al., 2014). This heating contrast between the anomalously warmer summer hemisphere and the anomalously colder winter hemisphere generates dynamical responses in atmospheric circulation (Lee & Poulsen, 2005; Raymo & Nisancioglu, 2003). In order to balance the changes in incoming energy, there is a strengthening in the Hadley Cell of the winter hemisphere during maximum obliquity. This strengthening increases the cross-equatorial moisture transport into the summer hemisphere, pushes the ITCZ towards the summer hemisphere and increases the strength of trade winds in the winter hemisphere (Lee & Poulsen, 2005; Liu & Yang, 2003; Mantsis et al., 2014). This phenomenon had a marked influence in the North African and Asian monsoon systems (e.g., Caley et al. 2011; Caley, Roche, and Renssen 2014; Mantsis et al. 2014; Mohtadi, Prange, and Steinke 2016) for example, and may also have affected precipitation in other continents, albeit in a less intense way. Indeed, over eastern tropical South America (where the SFRB is located), modelling studies have shown that maximum obliquity triggers a slight increase in austral winter precipitation (Bosmans et al., 2015) due to a strengthening of the SE trade winds that transport more South Atlantic moisture into eastern tropical South America (Liu & Yang, 2003). An opposite response (i.e., a decrease in austral winter precipitation over eastern tropical South America) is expected for austral winter under minimum obliquity. The difference in winter precipitation between maximum and minimum obliquity was, however, expected to be small (Bosmans et al., 2015).

Our $\delta^{13}C_{wax}$ record indicates that the distribution of C3 versus C4 vegetation in the SFRB during the last ca. 45 kyr follows obliquity (Figure 3.3c, d), with extended C4 vegetation (i.e., savanna and grasslands) under minimum obliquity (ca. 29 ka BP) and extended C3 vegetation (i.e., tropical forest) under maximum obliquity (ca. 15 ka BP). We suggest that this savanna and grasslands to tropical forest shift is related to a gradual decrease in DSL. A decrease in the DSL over the SFRB from ca. 29 to 15 ka BP was produced by the slight increase in austral winter precipitation, an effect of the strengthening Hadley Cell and SE trade winds, both triggered by an increase in obliquity.

In order to test our suggestion that DSL is able to control the extent of tropical forest (C3) versus savanna and grasslands (C4) vegetation in the SFRB, we compared the modern distribution of these biomes (Souza et al., 2020) to instrumental DSL data (Funk et al., 2015) from the area 7-22°S, 48-36°W that encompasses the SFRB (Figure 3.4). Our results indicate that both savanna and grasslands and tropical forest are likely to occur for mean annual precipitation values above 1000 mm/yr, and the predominance of one or the other biome depends on the DSL. We find that in areas dominated by tropical forests the median DSL is 7.0 months, while in areas dominated by savanna and grasslands the median DSL is 7.4 months. This indicates that a higher DSL increase the stability of savanna and grasslands, and that even a small decrease (increase) in DSL is enough to foster the spread of tropical forest (savanna and grasslands) in the SFRB. Thus, our suggestion based on downcore data (Figure 3.3d) finds support on the modern distribution of tropical forest and savanna and grasslands over the SFRB region. Importantly, the change in mean annual precipitation due to the varying DSL during the last ca. 45 kyr is small, otherwise our δD_{wax} values as well as SFRB speleothem $\delta^{18}O$ and marine sediment core ln(Ti/Ca) values (Campos et al., 2019; Stríkis et al., 2011, 2018) would have recorded it.

3.6.2 Millennial forcing

Millennial-scale precipitation anomalies in the SFRB are well described in the literature (Campos et al., 2019; Stríkis et al., 2015, 2018). According to Campos et al. (2019), positive precipitation anomalies over the SFRB during HS are associated with increased austral summer rainfall over eastern tropical South America due to an anomalous cyclonic circulation and moisture transport from the warmer South Atlantic into the continent.

Indeed, our δD_{wax} record indicates increases in precipitation over the SFRB during HS4-HS1 (Figure 3.3). The new record bears some advantages in relation to previously existing hydroclimate indicators. First, the ln(Ti/Ca) data used in Campos et al. (2019) to infer changes in precipitation in the SFRB is essentially an erosion indicator (Govin et al., 2012). Second, speleothem $\delta^{18}O$ used in Stríkis et al. (2015, 2018) register conditions at the specific location of the sampled caves. Instead, our δD_{wax} data is a direct indicator of precipitation and provides a basin-integrated signal.

Our $\delta^{13}C_{wax}$ data suggest that millennial scale changes in vegetation in the SFRB are modulated by obliquity, and different HS show a distinct response depending on the obliquity phase (Figure 3.3). HS4 and HS1 occurred during high obliquity when DSL was short. Under this obliquity configuration, increased austral summer precipitation led to a tropical forest (C3) spread trough the basin. On the other hand, HS3 and HS2 occurred during low obliquity, when DSL was long. This obliquity configuration led to a savanna and grasslands (C4) spread even under increased austral summer precipitation. The distinct responses of vegetation to increases in austral summer precipitation (and mean annual precipitation) corroborate our suggestion that the DSL is an important factor governing the long-term distribution of tropical forest versus savanna and grasslands in eastern tropical South America.

3.6.3 Ecological perspectives

Past obliquity-induced changes in the intrahemispheric meridional insolation gradient (and, consequently, in the surface temperature gradient) bear similarities to projected changes in the intrahemispheric meridional surface temperature gradient due to global warming (Mantsis et al., 2014). Indeed, climate models indicate a widening and weakening of the Hadley Cell by the end of the century (Collins et al., 2013; Lu et al., 2008), that bear similarities to past periods of minimum obliquity (Mantsis et al., 2014). It is also expected that the contrast between wet and dry seasons will increase over most parts of the globe (Collins et al., 2013). In the SFRB region, projections indicate an increase in droughts and aridity, as well as an intensification in the vulnerability of the semiarid northeastern Brazil (Marengo et al., 2017; Marengo & Bernasconi, 2015).

These anticipated changes will likely increase the DSL regionally, negatively affecting the distribution of trees. One such change can be sudden and occur in a not easily reversible way (Staver et al., 2011a). Despite being an urgent matter (Hirota & Oliveira, 2020), the factors that govern the transition and stability between tropical forest and savanna are still largely unknown (Bond, 2008; Hoffmann et al., 2012a; House et al., 2003; Ratnam et al., 2011). To what extent mean annual rainfall, seasonality in rainfall, fire occurrence, topography, herbivore activity and soil fertility control the occurrence of these biomes is an open question.

The space-for-time substitution consists of predicting ecological time-series by the analysis of spatially separate sites based on either ecological or environmental gradients (Blois et al., 2013; Fukami & Wardle, 2005; Pickett, 1989). It is commonly used to infer long-term dynamics in applied ecology. Despite its advantages, it has been suggested that this approach can greatly underestimate the consequences that environmental stressors have on the diversity of species and on the renewal of communities (França et al., 2016). Paleoenvironmental records, as our $\delta^{13}C_{wax}$, provide a long-term perspective on understanding the controls, magnitudes and spatial/temporal aspects of ecological changes, circumventing the limitations of the space-for-time substitution (Pancost, 2017).

Fire has been hypothesized to play an important role in the distribution of savannas (Bond, 2008; Staver et al., 2011a). We propose that under minimum obliquity (e.g., ca. 29 ka BP), the increase in the DSL produced favorable conditions for fire occurrence (i.e., increased grass layer), resulting in a positive feedback to the expansion of savanna and grasslands initially triggered by the longer DSL. On the other hand, under maximum obliquity (ca. 15 ka BP), the shorter DSL increased tree density and decreased the grass layer, greatly hindering flammability (Hoffmann et al., 2012b). We provide a climatic mechanism that justifies the variation of DSL in the long-term, which, in turn, governed biome shifts in eastern tropical South America both directly and indirectly, through fire activity.

3.7 CONCLUSIONS

Our long-chain *n*-alkanes $\delta^{13}C$ and δD results show that eastern tropical South America experienced vegetational and hydrological changes both in orbital and millennial timescales during the last ca. 45 kyr. The $\delta^{13}C$ record shows a marked obliquity pacing but varying responses in the millennial-scale variability. On the other hand, the δD record shows no orbital signal but clear negative excursions during Heinrich Stadials. For the first time, we describe that obliquity influences vegetation change in eastern tropical South America through its control on the dry season length. On orbital timescale, an increase in obliquity leads to a decrease in the dry season length, that triggers an expansion of tree coverage. The opposite situation is valid for a decrease in obliquity. On millennial-scale, we show that increases in mean annual precipitation over eastern tropical South America produced varying responses in vegetation, depending on the obliquity configuration. Under maximum (minimum) obliquity and its associated decreased (increased) dry season length, millennial-scale increases in precipitation fostered the expansion of tree (grass) cover.

3.8 ACKNOWLEDGEMENTS

Logistic and technical assistance was provided by the captain and crew of the R/V Meteor. New data shown herein will be archived in Pangaea. J. Q. Ferreira acknowledges the financial support from Coordenação de Aperfeiçoamento de Pessoal de Nível Superior (CAPES) (grant 88882.328049/2019-01). C. M. Chiessi acknowledges the financial support from FAPESP (grants 2018/15123-4 and 2019/24349-9), CAPES (grants 564/2015 and 88881.313535/2019-01), Conselho Nacional de Desenvolvimento Científico e Tecnológico (CNPq) (Grant 302607/2016-1), and the Alexander von Humboldt-Stiftung. We thank Ralph Kreutz for the technical support in the analyzes of plant waxes.

3.9 SUPPLEMENTARY MATERIAL

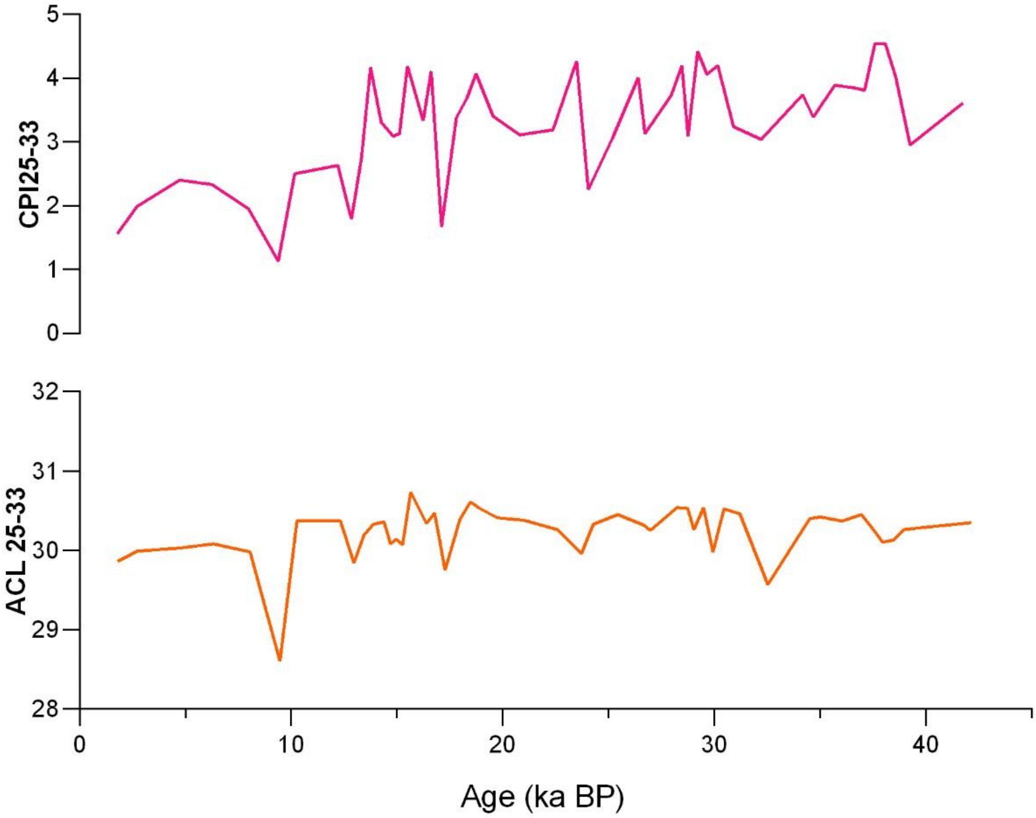

Figure S1. Downcore records of the carbon preference index (CPI_{25-33}) and the average chain length (ACL_{25-33}) of marine sediment core M125-95-3 for the last ca. 45 kyr. Despite the low Holocene CPI_{25-33} values, the long-chain *n*-alkanes present in most of the record are predominantly derived from terrestrial higher plants (Cranwell, 1981).

4 CHAPTER 4

4.1 CONCLUSIONS

The investigation of the long-chain *n*-alkanes from a marine sediment core collected off the mouth of the São Francisco River allowed a better understanding of the major hydrological and vegetational changes that occurred in the SFRB during the last ca. 45 kyr. From this, our main conclusions are:

I. The δD and $\delta^{13}C$ composition of plant-wax *n*-alkanes are useful tools for the reconstruction of the amount of precipitation and the dominant vegetation type (i.e., C3 versus C4), respectively, in the SFRB.

II. Despite the strong control that precession exerts over the strength of the SAMS, neither our δD_{wax} nor our $\delta^{13}C_{wax}$ records show this type of orbital pacing.

III. Our δD_{wax} data show no orbital pacing at all.

IV. Our δD_{wax} record indicates increases in precipitation over the SFRB during HS4-HS1. For the first time, a basin-integrated signal from a direct precipitation indicator is provided.

V. Our $\delta^{13}C_{wax}$ record shows a prominent obliquity pacing. For the first time, we show that obliquity influences vegetation dynamics in eastern tropical South America through its control of the DSL. We suggest that periods of maximum (minimum) obliquity increased (decreased) the intra-hemispheric insolation gradient during austral winter, strengthening the austral Hadley circulation and the southeastern trade winds. These processes slightly increased winter precipitation over the São Francisco river drainage basin, decreasing the length of the dry season.

VI. Our $\delta^{13}C_{wax}$ record also shows variability in response to millennial-scale climate change events. Different HS show a distinct response depending on the obliquity phase. HS4 and HS1 occurred during high obliquity when DSL was short, which led to a C3 spread over the basin. HS3 and HS2, on the other hand, occurred during low obliquity, when DSL was long, which led to C4 spread over the basin.

REFERENCES

ANA - Agência Nacional de Águas - Superintendência de Planejamento de Recursos Hídricos. (2015). **Conjuntura dos recursos hídricos no Brasil: regiões hidrográficas brasileiras** – Edição Especial.

AZEVEDO, J. A. R., COLLEVATTI, R. G., JARAMILLO, C. A., STRÖMBERG, C. A. E., GUEDES, T. B., MATOS-MARAVÍ, P., BACON, C. D., CARILLO, J. D., FAURBY, S., & ANTONELLI, A. (2020). **On the Young Savannas in the Land of Ancient Forests**, 271–298.

BAHR, A., ALBUQUERQUE, A., ARDENGHI, N., BATENBURG, S., BAYER, M., CATUNDA, M.C., CONFORTI, A., DIAS, B., RAMOS, R.D., EGGER, L.M., EVERS, F., FISCHER, T., HATSUKANO, K., HENNRICH, B., HOFFMANN, J., JIVCOV, S., KUSCH, S., MUNZ, P., NIEDERMEYER, E., OSBORNE, A., RADDATZ, J., RAEKE, A., REISSIG, S., SEBASTIAN, U., TANIGUCHI, N., & VENANCIO, I. (2016). **South American Hydrological Balance and Paleoceanography during the Late Pleistocene and Holocene (SAMBA) – Cruise No. M125**, March 21 – April 15, 2016 - Rio de Janeiro (Brazil) – Fortaleza (Brazil).

BEHLING, H., W. ARZ, H., PÄTZOLD, J., & WEFER, G. (2000). Late Quaternary vegetational and climate dynamics in northeastern Brazil, inferences from marine core GeoB 3104-1. **Quaternary Science Reviews**, 19(10), 981–994.

BEHLING, H. (2003). Late glacial and Holocene vegetation, climate and fire history inferred from Lagoa Nova in the southeastern Brazilian lowland. **Vegetation History and Archaeobotany**, 12(4), 263–270.

BINTANJA, R., VAN DE WAL, R. & OERLEMANS, J. (2005) Modelled atmospheric temperatures and global sea levels over the past million years. **Nature,** 437, 125–128.

BLAAUW, M., & CHRISTENY, J. A. (2011). Flexible paleoclimate age-depth models using an autoregressive gamma process. **Bayesian Analysis**, 6(3), 457–474.

BLOIS, J. L., WILLIAMS, J. W., FITZPATRICK, M. C., JACKSON, S. T., & FERRIER, S. (2013). Space can substitute for time in predicting climate-change effects on biodiversity**. Proceedings of the National Academy of Sciences of the United States of America**, 110(23), 9374–9379.

BOND, G., HEINRICHT, H., BROECKER, W., LABEYRIE, L., MCMANUS, J., ANDREWS, J., HUONLL, S., JANTSCHIK, R., CLASEN, S., SIMET, C., TEDESCO, K., KLAS, M., BONANITT, G., & IVY, S. (1992). **Letters to nature,** 15(360), 1668–1672.

BOND, W. J. (2005). Large parts of the world are brown or black: A different view on the “Green World” hypothesis. **Journal of Vegetation Science**, 16(3), 261–266.

BOND, W. J. (2008). What limits trees in C4 grasslands and savannas? **Annual Review of Ecology, Evolution, and Systematics**, 39, 641–659.

BOND, W. J., & KEELEY, J. E. (2005). Fire as a global “herbivore”: The ecology and evolution of flammable ecosystems. **Trends in Ecology and Evolution**, 20(7), 387–394.

BOSMANS, J. H. C., HILGEN, F. J., TUENTER, E., & LOURENS, L. J. (2015). Obliquity forcing of low-latitude climate. **Climate of the Past**, 11(10), 1335–1346.

BOUIMETARHAN, I., CHIESSI, C. M., GONZÁLEZ-ARANGO, C., DUPONT, L., VOIGT, I., PRANGE, M., & ZONNEVELD, K. (2018). Intermittent development of forest corridors in northeastern Brazil during the last deglaciation: Climatic and ecologic evidence. **Quaternary Science Reviews**, 192, 86–96.

BRIDGEWATER, S., RATTER, J. A., & FELIPE RIBEIRO, J. (2004). Biogeographic patterns, -diversity and dominance in the cerrado biome of Brazil. **Biodiversity and Conservation**, 13(12), 2295–2317.

BUSH, R. T., & MCINERNEY, F. A. (2013). Leaf wax *n*-alkane distributions in and across modern plants: Implications for paleoecology and chemotaxonomy. **Geochimica et Cosmochimica Acta**, 117, 161–179.

BUTZIN, M., KÖHLER, P., & LOHMANN, G. (2017). Marine radiocarbon reservoir age simulations for the past 50,000 years. **Geophysical Research Letters**, 44(16), 8473–8480.

CALEY, T., MALAIZÉ, B., REVEL, M., DUCASSOU, E., WAINER, K., IBRAHIM, M., SHOEAIB, D., MIGEON, S., & MARIEU, V. (2011). Orbital timing of the Indian, East Asian and African boreal monsoons and the concept of a "global monsoon." **Quaternary Science Reviews**, 30(25–26), 3705–3715.

CALEY, T., ROCHE, D. M., & RENSSEN, H. (2014). Orbital Asian summer monsoon dynamics revealed using an isotope-enabled global climate model. **Nature Communications**, 5, 6–11.

CAMPOS, M. C., CHIESSI, C. M., PRANGE, M., MULITZA, S., KUHNERT, H., PAUL, A., VENANCIO, I. M., ALBUQUERQUE, A. L. S., CRUZ, F. W., & BAHR, A. (2019). A new mechanism for millennial scale positive precipitation anomalies over tropical South America. **Quaternary Science Reviews**, 225.

CARVALHO, L. M. V., JONES, C., & LIEBMANN, B. (2004). The South Atlantic convergence zone: Intensity, form, persistence, and relationships with intraseasonal to interannual activity and extreme rainfall. **Journal of Climate**, 17(1), 88–108.

CASSINO, R. F., LEDRU, M. P., SANTOS, R. DE A., & FAVIER, C. (2020). Vegetation and fire variability in the central Cerrados (Brazil) during the Pleistocene-Holocene transition was influenced by oscillations in the SASM boundary belt. **Quaternary Science Reviews**, 232, 106209.

CASSINO, R. F., MARTINHO, C. T., & DA SILVA CAMINHA, S. A. F. (2018). A Late Quaternary palynological record of a palm swamp in the Cerrado of central Brazil interpreted using modern analog data. **Palaeogeography, Palaeoclimatology, Palaeoecology**, 490, 1–16.

CASSINO, R., & MEYER, K. E. B. (2013). Reconstituição paleoambiental do chapadão dos gerais (Quaternário tardio) a partir da análise palinológica da vereda Laçador, Minas Gerais, Brasil. **Revista Brasileira de Paleontologia**, 16(1), 127–146.

CASTAÑEDA, I. S., & SCHOUTEN, S. (2011). A review of molecular organic proxies for examining modern and ancient lacustrine environments. **Quaternary Science Reviews**, 30(21–22), 2851–2891.

CHENG, H., SINHA, A., CRUZ, F. W., WANG, X., EDWARDS, R. L., D'HORTA, F. M., RIBAS, C. C., VUILLE, M., STOTT, L. D., & AULER, A. S. (2013). Climate change patterns in Amazonia and biodiversity. **Nature Communications**, 4.

COLLINS, M., R. KNUTTI, J. ARBLASTER, J.-L. DUFRESNE, T. FICHEFET, P. FRIEDLINGSTEIN, X. GAO, W.J. GUTOWSKI, T. JOHNS, G. KRINNER, M. SHONGWE, C. TEBALDI, A. J. W. AND M. W. (2013). **Long-term Climate Change: Projections, Commitments and Irreversibility Pages 1029 to 1076**. In Intergovernmental Panel on Climate Change (Ed.), Climate Change 2013 - The Physical Science Basis (Vol. 9781107057, pp. 1029–1136). Cambridge University Press.

COLLINS, J. A., PRANGE, M., CALEY, T., GIMENO, L., BECKMANN, B., MULITZA, S., SKONIECZNY, C., ROCHE, D., & SCHEFUß, E. (2017). Rapid termination of the African Humid Period triggered by northern high-latitude cooling. **Nature Communications**, 8(1).

CRUZ, F. W., BURNS, S. J., KARMANN, I., SHARP, W. D., VUILLE, M., CARDOSO, A. O., FERRARI, J. A., SILVA DIAS, P. L., & VIANA, O. (2005). Insolation-driven changes in atmospheric circulation over the past 116,000 years in subtropical Brazil. **Nature**, 434(7029), 63–66.

CRUZ, F. W., VUILLE, M., BURNS, S. J., WANG, X., CHENG, H., WERNER, M., LAWRENCE EDWARDS, R., KARMANN, I., AULER, A. S., & NGUYEN, H. (2009). Orbitally driven east-west antiphasing of South American precipitation. **Nature Geoscience**, 2(3), 210–214.

DANSGAARD, W. (1964). Stable isotopes in precipitation. Tellus, 16(4), 436–468.

DA SILVA, J. M. C., & BATES, J. M. (2002). Biogeographics patterns and coservation in the South American Cerrado: A tropical savanna hotspot. **BioScience**, 52(3), 225–233.

DE OLIVEIRA, P. E., BARRETO, A. M. F., & SUGUIO, K. (1999). Late Pleistocene/Holocene climatic and vegetational history of the Brazilian caatinga: The fossil dunes of the middle Sao Francisco River. **Palaeogeography, Palaeoclimatology, Palaeoecology**, 152(3–4), 319–337.

DIEFENDORF, A. F., & FREIMUTH, E. J. (2017). Extracting the most from terrestrial plant-derived n-alkyl lipids and their carbon isotopes from the sedimentary record: A review. **Organic Geochemistry,** (103), 1–21.

DUPONT, L. M., SCHLÜTZ, F., EWAH, C. T., JENNERJAHN, T. C., PAUL, A., & BEHLING, H. (2010). Two-step vegetation response to enhanced precipitation in Northeast Brazil during Heinrich event 1. **Global Change Biology**, 16(6), 1647–1660.

EGLINTON, G., & HAMILTON, R. J. (1967). Leaf epicuticular waxes. **Science**, 156(3780), 1322–1335.

FRANÇA, F., LOUZADA, J., KORASAKI, V., GRIFFITHS, H., SILVEIRA, J. M., & BARLOW, J. (2016). Do space-for-time assessments underestimate the impacts of logging on tropical biodiversity? An Amazonian case study using dung beetles. **Journal of Applied Ecology**, 53(4), 1098–1105.

FUKAMI, T., & WARDLE, D. A. (2005). Long-term ecological dynamics: Reciprocal insights from natural and anthropogenic gradients. Proceedings of the Royal Society B: **Biological Sciences**, 272(1577), 2105–2115.

FUNK, C., PETERSON, P., LANDSFELD, M., PEDREROS, D., VERDIN, J., SHUKLA, S., HUSAK, G., ROWLAND, J., HARRISON, L., HOELL, A., & MICHAELSEN, J. (2015). The climate hazards infrared precipitation with stations - A new environmental record for monitoring extremes. **Scientific Data**, 2, 1–21.

GARCIN, Y., SCHEFUß, E., SCHWAB, V. F., GARRETA, V., GLEIXNER, G., VINCENS, A., TODOU, G., SÉNÉ, O., ONANA, J. M., ACHOUNDONG, G., & SACHSE, D. (2014). Reconstructing C3 and C4 vegetation cover using n-alkane carbon isotope ratios in recent lake sediments from Cameroon, Western Central Africa. **Geochimica et Cosmochimica Acta,** 142, 482–500.

GARREAUD, R. D., VUILLE, M., COMPAGNUCCI, R., & MARENGO, J. (2009). Present-day South American climate. **Palaeogeography, Palaeoclimatology, Palaeoecology**, 281(3–4), 180–195.

GOMES, H. B., AMBRIZZI, T., HERDIES, D. L., HODGES, K., & PONTES DA SILVA, B. F. (2015). Easterly wave disturbances over Northeast Brazil: An observational analysis. **Advances in Meteorology**, 2015.

GOVIN, ALINE, HOLZWARTH, U., HESLOP, D., FORD KEELING, L., ZABEL, M., MULITZA, S., COLLINS, J. A., & CHIESSI, C. M. (2012). Distribution of major elements in Atlantic surface sediments (36°N-49°S): Imprint of terrigenous input and continental weathering. **Geochemistry, Geophysics, Geosystems**, 13(1).

GOVIN, A., CHIESSI, C. M., ZABEL, M., SAWAKUCHI, A. O., HESLOP, D., HÖRNER, T., ZHANG, Y., & MULITZA, S. (2014). Terrigenous input off northern South America driven by changes in Amazonian climate and the North Brazil Current retroflection during the last 250 ka. **Climate of the Past**, 10(2), 843–862.

GRACE, J., JOSÉ, J. S., MEIR, P., MIRANDA, H. S., & MONTES, R. A. (2006). Productivity and carbon fluxes of tropical savannas. **Journal of Biogeography**, 33(3), 387–400.

HÄGGI, C., SAWAKUCHI, A. O., CHIESSI, C. M., MULITZA, S., MOLLENHAUER, G., SAWAKUCHI, H. O., BAKER, P. A., ZABEL, M., & SCHEFUß, E. (2016). Origin, transport and deposition of leaf-wax biomarkers in the Amazon Basin and the adjacent Atlantic. **Geochimica et Cosmochimica Acta**, 192, 149–165.

HÄGGI, C., CHIESSI, C. M., MERKEL, U., MULITZA, S., PRANGE, M., SCHULZ, M., & SCHEFUß, E. (2017). Response of the Amazon rainforest to late Pleistocene climate variability. **Earth and Planetary Science Letters**, 479, 50–59.

HARRIS, I., OSBORN, T. J., JONES, P., & LISTER, D. (2020). Version 4 of the CRU TS monthly high-resolution gridded multivariate climate dataset. **Scientific Data**, 7(1), 1–18.

HASTENRATH, S. (2012). **Exploring the climate problems of Brazil's Nordeste: A review**. In Climatic Change (Vol. 112, Issue 2, pp. 243–251). Springer.

HEINRICH, H. (1988). Origin and consequences of cyclic ice rafting in the Northeast Atlantic Ocean during the past 130,000 years. **Quaternary Research**, 29(2), 142–152.

HENNENBERG, K. J., FISCHER, F., KOUADIO, K., GOETZE, D., ORTHMANN, B., LINSENMAIR, K. E., JELTSCH, F., & POREMBSKI, S. (2006). Phytomass and fire occurrence along forest-savanna transects in the Comoé National Park, Ivory Coast. **Journal of Tropical Ecology**, 22(3), 303–311.

HIROTA, M., NOBRE, C., OYAMA, M. D., & BUSTAMANTE, M. M. C. (2010). The climatic sensitivity of the forest, savanna and forest-savanna transition in tropical South America. **New Phytologist**, 187(3), 707–719.

HIROTA, M., HOLMGREN, M., VAN NES, E. H., & SCHEFFER, M. (2011). Global Resilience of Tropical Forest. **Science**, 334(October), 232–235.

HIROTA, M., & OLIVEIRA, R. (2020). Crossing thresholds on the way to ecosystem shifts. **Science**, 367(6479), 739–740.

HOFFMANN, W. A., GEIGER, E. L., GOTSCH, S. G., ROSSATTO, D. R., SILVA, L. C. R., LAU, O. L., HARIDASAN, M., & FRANCO, A. C. (2012). Ecological thresholds at the savanna-forest boundary: How plant traits, resources and fire govern the distribution of tropical biomes. **Ecology Letters**, 15(7), 759–768.

HOFFMANN, W. A., JACONIS, S. Y., MCKINLEY, K. L., GEIGER, E. L., GOTSCH, S. G., & FRANCO, A. C. (2012b). Fuels or microclimate? Understanding the drivers of fire feedbacks at savanna-forest boundaries. **Austral Ecology**, 37(6), 634–643.

HORÁK-TERRA, I., CORTIZAS, A. M., DA LUZ, C. F. P., SILVA, A. C., MIGHALL, T., DE CAMARGO, P. B., MENDONÇA-FILHO, C. V., DE OLIVEIRA, P. E., CRUZ, F. W., & VIDAL-TORRADO, P. (2020). Late Quaternary vegetation and climate dynamics in central-eastern Brazil: insights from a ~35k cal a bp peat record in the Cerrado biome. **Journal of Quaternary Science**, 35(5), 664–676.

HOU, A., BAHR, A., RADDATZ, J., VOIGT, S., GREULE, M., ALBUQUERQUE, A. L., CHIESSI, C. M., & FRIEDRICH, O. (2020). Insolation and Greenhouse Gas Forcing of the South American Monsoon System Across Three Glacial-Interglacial Cycles. **Geophysical Research Letters**, 47(14), 1–10.

HOUSE, J. I., ARCHER, S., BRESHEARS, D. D., SCHOLES, R. J., TREE, N., INTERACTIONS, G., & MAX, P. (2003). **Conundrums in mixed woody – herbaceous**

plant systems. 1763–1777.

HUANG. (2001). Climate Change as the Dominant Control on Climate Change as the Dominant Control on Glacial-Interglacial Variations in C 3 and C 4 Plant Abundance. **Science**, 1647(2001), 1647–1651.

HUYBERS, P. (2006). Early pleistocene glacial cycles and the integrated summer insolation forcing. **Science**, 313(5786), 508–511.

HUYBERS, P. (2007). Glacial variability over the last two million years: an extended depth-derived agemodel, continuous obliquity pacing, and the Pleistocene progression. **Quaternary Science Reviews**, 26(1–2), 37–55.

IBGE. (2004). Map of Brazilian Biomes, Scale 1:500000. Instituto Brasileiro de Geografia e Estatística. Rio de Janeiro, Brazil.

JACKSON, R. B., BANNER, J. L., JOBBÁGY, E. G., POCKMAN, W. T., & WALL, D. H. (2002). Ecosystem carbon loss with woody plant invasion of grasslands. **Nature**, 418(6898), 623–626.

JENNERJAHN, T. C., ITTEKKOT, V., ARZ, H. W., & BEHLING, H. (2004). Asynchronous Terrestrial and Marine Signals of Climate Change During Heinrich Events. **Science**, 306, 2236-2239.

KOUSKY, V. E. (1979). Frontal influences on northeast Brazil. **Monthly Weather Review**, 107(9), 1140–1153.

LANGNER, M., & MULITZA, S. (n.d.). **Technical Note: PaleoDataView-A software toolbox for the collection, homogenization and visualization of marine proxy data**.

LASKAR, J., ROBUTEL, P., JOUTEL, F., GASTINEAU, M., CORREIA, A. C. M., & LEVRARD, B. (2004). A long-term numerical solution for the insolation quantities of the Earth. **Astronomy and Astrophysics**, 428(1), 261–285.

LEDRU, M. P. (1993). Late Quaternary Environmental and Climatic Changes in Central Brazil. **Quaternary Research,** 39(1), 90–98.

LEE, S. Y., & POULSEN, C. J. (2005). Tropical Pacific climate response to obliquity forcing in the Pleistocene. **Paleoceanography**, 20(4), 1–10.

LENTERS, J. D., & COOK, K. H. (1997). On the origin of the Bolivian high and related circulation features of the South American climate. **Journal of the Atmospheric Sciences**, 54(5), 656–677.

LIU, Z., & YANG, H. (2003). Extratropical control of tropical climate, the atmospheric bridge and oceanic tunnel. **Geophysical Research Letters**, 30(5), n/a-n/a.

LLOYD, J., BIRD, M. I., VELLEN, L., MIRANDA, A. C., VEENENDAAL, E. M., DJAGBLETEY, G., MIRANDA, H. S., COOK, G., & FARQUHAR, G. D. (2008). Contributions of woody and herbaceous vegetation to tropical savanna ecosystem productivity: A quasi-global estimate. **Tree Physiology**, 28(3), 451–468.

LU, J., CHEN, G., & FRIERSON, D. M. W. (2008). Response of the zonal mean atmospheric circulation to El Niño versus global warming. **Journal of Climate**, 21(22), 5835–5851.

MANTSIS, D. F., LINTNER, B. R., BROCCOLI, A. J., ERB, M. P., CLEMENT, A. C., & PARK, H. S. (2014). The response of large-scale circulation to obliquity-induced changes in meridional heating gradients. **Journal of Climate**, 27(14), 5504–5516.

MARENGO, J. A. (2001). **Mudancas climáticas globais e regionais**. In Revista Brasileira de Meteorologia (Vol. 16, pp. 1–18).

MARENGO, J. A., & BERNASCONI, M. (2015). Regional differences in aridity/drought conditions over Northeast Brazil: present state and future projections. **Climatic Change**, 129(1–2), 103–115.

MARENGO, J. A., TORRES, R. R., & ALVES, L. M. (2017). Drought in Northeast Brazil—past, present, and future. **Theoretical and Applied Climatology**, 129(3–4), 1189–1200.

MARSHALL, J., DONOHOE, A., FERREIRA, D. ET AL. (2014) The ocean's role in setting the mean position of the Inter-Tropical Convergence Zone. **Climate Dynamics** 42, 1967–1979.

MENDONÇA, L. A. R., FRISCHKORN, H., SANTIAGO, M. F., DE CAMARGO, P. B., DE LIMA, J. O. G., & FILHO, J. M. (2010). Identification of forest changes using 13C and 15N of soils of the Araripe Plateau, Ceará. **Revista Brasileira de Engenharia Agricola e Ambiental**, 14(3), 314–319.

MENDES, V., SAWAKUCHI, A. O., M. CHIESSI, C., F. GIANNINI, P. C., REHFELD, K., & MULITZA, S. (2019). Thermoluminescence and Optically Stimulated Luminescence Measured in Marine Sediments Indicate Precipitation Changes Over Northeastern Brazil. **Paleoceanography and Paleoclimatology**, 34(8), 1476–1486.

MEYERS, P. A. (1997). Organic geochemical proxies of paleoceanographic, paleolimnologic, and paleoclimatic processes. **Organic Geochemistry**, 27(5–6), 213–250.

MEYERS, P. A. (2003). Applications of organic geochemistry to paleolimnological reconstructions: A summary of examples from the Laurentian Great Lakes. **Organic Geochemistry**, 34(2), 261–289.

MOHTADI, M., PRANGE, M., & STEINKE, S. (2016). Palaeoclimatic insights into forcing and response of monsoon rainfall. **Nature**, 533(7602), 191–199.

MULITZA, S., CHIESSI, C. M., SCHEFUß, E., LIPPOLD, J., WICHMANN, D., ANTZ, B., MACKENSEN, A., PAUL, A., PRANGE, M., REHFELD, K., WERNER, M., BICKERT, T., FRANK, N., KUHNERT, H., LYNCH-STIEGLITZ, J., PORTILHO-RAMOS, R. C., SAWAKUCHI, A. O., SCHULZ, M., SCHWENK, T., … ZHANG, Y. (2017). Synchronous and proportional deglacial changes in Atlantic meridional overturning and northeast Brazilian precipitation. **Paleoceanography**, 32(6), 622–633.

MYERS, N., MITTERMEIER, R. A., MITTERMEIER, C. G., DA FONSECA, G. A. B., & KENT, J. (2000). Biodiversity hotspots for conservation priorities. **Nature**, 403(6772), 853–858.

O'LEARY, M. H. (1988). Carbon isotopes in photosynthesis. **BioScience**, 38(5), 328–336.

OLIVEIRA-FILHO, A. T., & FONTES, M. A. L. (2000). Patterns of Floristic Differentiation among Atlantic Forests in Southeastern Brazil and the Influence of Climate1. **Biotropica**, 32(4b), 793–810.

PANCOST, R. D. (2017). Climate change narratives. **Nature Geoscience**, 10(7), 466–468.

PAUSAS, J. G., & BOND, W. J. (2020). Alternative Biome States in Terrestrial Ecosystems. **Trends in Plant Science**, 25(3), 250–263.

PESSENDA, L. C.R., ARAVENA, R., MELFI, A. J., TELLES, E. C. C., BOULET, R., VALENCIA, E. P. E., & TOMAZELLO, M. (1996). The use of carbon isotopes (^{13}C, ^{14}C) in soil to evaluate vegetation changes during the holocene in Central Brazil. **Radiocarbon**, 38(2), 191–201.

PESSENDA, L. C.R., GOMES, B. M., ARAVENA, R., RIBEIRO, A. S., BOULET, R., & GOUVEIA, S. E. M. (1998). The carbon isotope record in soils along a forest-cerrado ecosystem transect: Implications for vegetation changes in the Rondonia state, southwestern Brazilian Amazon region. **Holocene**, 8(5), 599–603.

PESSENDA, LUIZ CARLOS RUIZ, GOUVEIA, S. E. M., RIBEIRO, A. DE S., DE OLIVEIRA, P. E., & ARAVENA, R. (2010). Late Pleistocene and Holocene vegetation changes in northeastern Brazil determined from carbon isotopes and charcoal records in soils. **Palaeogeography, Palaeoclimatology, Palaeoecology**, 297(3–4), 597–608.

PICKETT, S. T. A. (1989). Space-for-Time Substitution as an Alternative to Long-Term Studies. **Long-Term Studies in Ecology**, 110–135

PORTILHO-RAMOS, R. C., CHIESSI, C. M., ZHANG, Y., MULITZA, S., KUCERA, M., SICCHA, M., PRANGE, M., & PAUL, A. (2017). Coupling of equatorial Atlantic surface stratification to glacial shifts in the tropical rainbelt. **Scientific Reports**, 7(1), 1–8.

PRADO, L. F., WAINER, I., & CHIESSI, C. M. (2013). Mid-Holocene PMIP3/CMIP5 model results: Intercomparison for the South American Monsoon System. **Holocene**, 23(12), 1915–1920.

PRADO, L. F., WAINER, I., CHIESSI, C. M., LEDRU, M. P., & TURCQ, B. (2013b). A mid-Holocene climate reconstruction for eastern South America. **Climate of the Past**, 9(5), 2117–2133.

RATNAM, J., BOND, W. J., FENSHAM, R. J., HOFFMANN, W. A., ARCHIBALD, S., LEHMANN, C. E. R., ANDERSON, M. T., HIGGINS, S. I., & SANKARAN, M. (2011). When is a "forest" a savanna, and why does it matter? **Global Ecology and Biogeography**, 20(5), 653–660.

RAYMO, M. E., & NISANCIOGLU, K. (2003). The 41 kyr world: Milankovitch's other unsolved mystery. **Paleoceanography**, 18(1), 1–6.

REIMER, P. J., EDOUARD BARD, B., ALEX BAYLISS, B., WARREN BECK, B. J., PAUL BLACKWELL, B. G., & CHRISTOPHER BRONK RAMSEY, B. (2013). Intcal13 and Marine13 Radiocarbon Age Calibration Curves 0–50,000 Years Cal Bp. **Radiocarbon**, 55(4), 1869–1887.

RIGINOS, C., & GRACE, J. B. (2008). Savanna tree density, herbivores, and the herbaceous community: Bottom-up vs. top-down effects. **Ecology**, 89(8), 2228–2238.

SACHSE, D., BILLAULT, I., BOWEN, G. J., CHIKARAISHI, Y., DAWSON, T. E., FEAKINS, S. J., FREEMAN, K. H., MAGILL, C. R., MCINERNEY, F. A., VAN DER MEER, M. T. J., POLISSAR, P., ROBINS, R. J., SACHS, J. P., SCHMIDT, H. L., SESSIONS, A. L., WHITE, J. W. C., WEST, J. B., & KAHMEN, A. (2012). Molecular paleohydrology: Interpreting the hydrogen-isotopic composition of lipid biomarkers from photosynthesizing organisms. **Annual Review of Earth and Planetary Sciences**, 40, 221–249.

SAMPAIO, E. V. S. B. (1995). **Overview of the Brazilian caatinga**. In Seasonally Dry Tropical Forests (pp. 35–63). Cambridge University Press.

SANCHEZ GOÑI, M. F., & HARRISON, S. P. (2010). Millennial-scale climate variability and vegetation changes during the Last Glacial: Concepts and terminology. **Quaternary Science Reviews**, 29(21–22), 2823–2827.

SANKARAN, M., RATNAM, J., & HANAN, N. P. (2004). Tree-grass coexistence in savannas revisited - Insights from an examination of assumptions and mechanisms invoked in existing models. **Ecology Letters**, 7(6), 480–490.

SCHEFUß, E., RATMEYER, V., STUUT, J. B. W., JANSEN, J. H. F., & SINNINGHE DAMSTÉ, J. S. (2003). Carbon isotope analyses of n-alkanes in dust from the lower atmosphere over the central eastern Atlantic. Geochimica et Cosmochimica Acta, 67(10), 1757–1767.

SCHEFUß, E., SCHOUTEN, S., & SCHNEIDER, R. R. (2005). Climatic controls on central African hydrology during the past 20,000 years. **Nature**, 437(7061), 1003–1006.

SCHEFUß, E., KUHLMANN, H., MOLLENHAUER, G., PRANGE, M., & PÄTZOLD, J. (2011). Forcing of wet phases in southeast Africa over the past 17,000 years. **Nature**, 480(7378), 509–512.

SCHNEIDER, T., BISCHOFF, T., & HAUG, G. H. (2014). Migrations and dynamics of the intertropical convergence zone. **Nature**, 513(7516), 45–53.

SCHOLES, R. J., & ARCHER, S. R. (1997). Tree-grass interactions in Savannas. **Annual Review of Ecology and Systematics**, 28(November), 517–544.

SCHRAG, D. P., ADKINS, J. F., MCINTYRE, K., ALEXANDER, J. L., HODELL, D. A., CHARLES, C. D., & MCMANUS, J. F. (2002). The oxygen isotopic composition of seawater during the Last Glacial Maximum. **Quaternary Science Reviews**, 21(1–3), 331–342.

SIMIONI, G., GIGNOUX, J., & LE ROUX, X. (2003). Tree layer spatial structure can affect savanna production and water budget: Results of a 3-D model. **Ecology**, 84(7), 1879–1894.

SMITH, F. A., & FREEMAN, K. H. (2006). Influence of physiology and climate on δD of leaf wax n-alkanes from C3 and C4 grasses. **Geochimica et Cosmochimica Acta**, 70(5), 1172–1187.

SOUZA, C. M., SHIMBO, J. Z., ROSA, M. R., PARENTE, L. L., ALENCAR, A. A., RUDORFF, B. F. T., HASENACK, H., MATSUMOTO, M., FERREIRA, L. G., SOUZA-FILHO, P. W. M., DE OLIVEIRA, S. W., ROCHA, W. F., FONSECA, A. V., MARQUES, C. B., DINIZ, C. G., COSTA, D., MONTEIRO, D., ROSA, E. R., VÉLEZ-MARTIN, E., … AZEVEDO, T. (2020). Reconstructing three decades of land use and land cover changes in brazilian biomes with landsat archive and earth engine. **Remote Sensing**, 12(17).

STAVER, A. C., ARCHIBALD, S., & LEVIN, S. (2011a). Tree cover in sub-Saharan Africa: Rainfall and fire constrain forest and savanna as alternative stable states. **Ecology**, 92(5), 1063–1072.

STAVER, A. C., ARCHIBALD, S., & LEVIN, S. A. (2011b). The global extent and determinants of savanna and forest as alternative biome states. **Science**, 334(6053), 230–232.

STRÍKIS, N. M., CHIESSI, C. M., CRUZ, F. W., VUILLE, M., CHENG, H., DE SOUZA BARRETO, E. A., MOLLENHAUER, G., KASTEN, S., KARMANN, I., EDWARDS, R. L., BERNAL, J. P., & SALES, H. D. R. (2015). Timing and structure of Mega-SACZ events during Heinrich Stadial 1. **Geophysical Research Letters**, 42(13), 5477–5484.

STRÍKIS, N. M., CRUZ, F. W., CHENG, H., KARMANN, I., EDWARDS, R. L., VUILLE, M., WANG, X., DE PAULA, M. S., NOVELLO, V. F., & AULER, A. S. (2011). Abrupt variations in South American monsoon rainfall during the Holocene based on a speleothem record from central-eastern Brazil. **Geology**, 39(11), 1075–1078.

STRÍKIS, N. M., CRUZ, F. W., BARRETO, E. A. S., NAUGHTON, F., VUILLE, M., CHENG, H., VOELKER, A. H. L., ZHANG, H., KARMANN, I., EDWARDS, R. L., AULER, A. S., SANTOS, R. V., & SALES, H. R. (2018). South American monsoon response to iceberg discharge in the North Atlantic. **Proceedings of the National Academy of Sciences**, 201717784.

TIERNEY, J. E., & DEMENOCAL, P. B. (2013). Abrupt shifts in Horn of Africa hydroclimate since the last glacial maximum. **Science**, 342(6160), 843–846.

TIPPLE, B. J., & PAGANI, M. (2007). The Early Origins of Terrestrial C 4 Photosynthesis. Annual Review of Earth and Planetary Sciences, 35(1), 435–461.

TOBY PENNINGTON, R., PRADO, D. E., & PENDRY, C. A. (2000). Neotropical seasonally dry forests and Quaternary vegetation changes. **Journal of Biogeography**, 27(2), 261–273.

TORRES, R. R., & FERREIRA, N. J. (2011). Case studies of easterly wave disturbances over

Northeast Brazil using the Eta Model. **Weather and Forecasting**, 26(2), 225–235.

VENANCIO, I. M., SHIMIZU, M. H., SANTOS, T. P., LESSA, D. O., PORTILHO-RAMOS, R. C., CHIESSI, C. M., CRIVELLARI, S., MULITZA, S., KUHNERT, H., TIEDEMANN, R., VAHLENKAMP, M., BICKERT, T., SAMPAIO, G., ALBUQUERQUE, A. L. S., VEIGA, S., NOBRE, P., & NOBRE, C. (2020). Changes in surface hydrography at the western tropical Atlantic during the Younger Dryas. **Global and Planetary Change**, 184, 103047.

VERA, C., HIGGINS, W., AMADOR, J., AMBRIZZI, T., GARREAUD, R., GOCHIS, D., GUTZLER, D., LETTENMAIER, D., MARENGO, J., MECHOSO, C. R., NOGUES-PAEGLE, J., SILVA DIAS, P. L., & ZHANG, C. (2006). Toward a unified view of the American monsoon systems. **Journal of Climate**, 19(20), 4977–5000.

WU, M. S., WEST, A. J., & FEAKINS, S. J. (2019). Tropical soil profiles reveal the fate of plant wax biomarkers during soil storage. Organic Geochemistry, 128, 1–15.

ZHANG, Y., CHIESSI, C. M., MULITZA, S., SAWAKUCHI, A. O., HÄGGI, C., ZABEL, M., PORTILHO-RAMOS, R. C., SCHEFUß, E., CRIVELLARI, S., & WEFER, G. (2017). Different precipitation patterns across tropical South America during Heinrich and Dansgaard-Oeschger stadials. **Quaternary Science Reviews**, 177, 1–9.

ZHOU, J., & LAU, K. M. (1998). Does a monsoon climate exist over South America? **Journal of Climate**, 11(5), 1020–1040.